MATRIX ISOLATION STUDIES ON TRANSITION METAL CARBONYLS AND RELATED SPECIES

JEREMY K. BURDETT

Department of Chemistry, University of Chicago, Chicago, Illinois, 60637 (U.S.A.)

CONTENTS

A. INTRODUCTION

The matrix isolation method [1] has been used for many years to study main group molecules and fragments with a small number of atoms, but studies of transition metal carbonyls and related species is a comparatively new field. It has proved to be a particularly productive area with a rich variety of interesting structural results and a fascinating photochemistry, both very sensitive to the *d* electron configuration of the transition metal complex concerned. Needless to say it has provided a useful testbed for theoretical ideas concerning transition metal systems and the utility of simple molecular orbital

treatments. It has also provided a novel approach to the study of heterogeneous catalytic processes.

Most of the studies we shall review involve carbonyl complexes, although N_2, O_2, NO, C_2H_4 and C_2H_2 are well represented. The carbonyl ligand is a particularly useful structural handle in transition metal chemistry. Vibrations in the infra-red around 2000 cm^{-1}, usually described as carbonyl stretches, are very intense. In the low-temperature matrix, rotational features are absent and the bands are very sharp. By a series of interesting coincidences to which we will refer later, the vibrational force field is well described by the high frequency approximation (neglect of all modes except $\nu(CO)$). This, combined with measurement of relative band intensities in the carbonyl stretching region, gives excellent quantitative estimates of the CMC bond angles in these systems. Similar spectroscopic features hold for the vibrational spectroscopy of the coordinated N_2 ligand which has been similarly exploited. No quantitative structural characterization or vibrational analysis has been performed to date for the NO ligand in a similar way. The O_2 ligand seems to prefer to bind in the sideways mode in the matrix studies we shall review, as does ethylene and acetylene in the majority of systems. Vibrational analyses of these latter systems has often been qualitative.

Infra-red (and to a lesser extent Raman) spectroscopy has dominated this field and given us the only quantitative structural results on species as diverse as AgO_2CO, $Ni(CO)_3$, $Fe(CO)_3$, $Ni(C_2H_4)$ and $Mo(CO)_5N_2$ which have either short or ultra short lifetimes under more 'normal' conditions. The carbonyls also have intense charge transfer electronic absorption bands in the UV region which although are perhaps of secondary interest from the point of view of structure determination, give rise to high efficiencies for photochemical reactions. These may be studied readily by the combination of UV/vis and carbonyl IR detection of the products of photolysis. In this review we shall discuss some of the structural and photochemical results obtained with carbonyls and related species in matrices, and also the relationship of some of the results to catalytic problems.

B. METHODS OF PRODUCTION OF NEW SPECIES

(i) The matrix isolation method

The principle behind the matrix isolation method is the following. If a reactive or unstable species is trapped in a rigid, chemically inert solid at low temperature then its lifetime may often be extended almost indefinitely. It is unable to diffuse through the solid matrix if the latter is rigid enough and the temperature sufficiently low, and will not therefore react with other species in the matrix. Only in exceptional circumstances, or by design as we see below will it react with the 'inert' matrix material itself. The only other possible decay pathway, unimolecular decomposition, may be blocked if the temperature is low compared with the activation energy for such a process. A schematic experimental arrangement is shown in Fig. 1 where the matrix is sup-
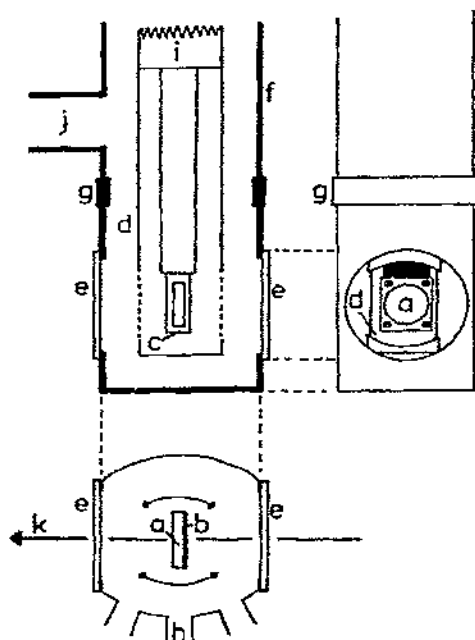
Fig. 1. Schematic diagram of the sample area of equipment used for matrix isolation studies in the IR to UV region of the spectrum: (a) low temperature window (usually KBr but other choices are necessary if low frequency IR bands are to be observed); (b) matrix; (c) window holder; (d) radiation shield; (e) outer windows (here again the choice of window material is dictated by spectral needs); (f) vacuum jacket; (g) rotatable seal allowing movement of central window relative to spray on ports; (h) spray on ports and holders of other equipment e.g. vacuum UV source, electron gun, metal atom source; (i) low temperature source (cryostat or closed cycle refrigerator); (j) pumping port; (k) path of IR or UV photolysis or detection beam.

ported on a salt window (usually CsI or KBr) clamped in a metal holder attached to a refrigeration source. This may be a dewar containing liquid H_2 (20 K) or liquid He (4 K) or, in recent years, a closed cycle refrigerator which can operate at any desired temperature from about 10 K upwards. The entire equipment is kept under high vacuum ($\sim 10^{-7}$ Torr) and the matrix may be spectroscopically examined by placing the whole cell in the sample beam of an IR or UV/vis spectrometer. The outer vacuum jacket which has two salt windows for such a spectral examination also contains ports for the introduction of matrix gas, metal atom sources, vacuum UV lamps etc.

An ideal matrix is one which is transparent in the regions needed for spectral examination, and the inert gases, methane and N_2 have been extensively used. These are transparent in the carbonyl stretching region of the IR and all through the visible and near UV. The matrix and the unstable species within it may be made in several ways.

(a) A stable molecule may be mixed with an excess of inert gas and depo-

sited on the sample window through one of the ports. The stable species may then be photolysed in situ and a new, perhaps unstable, species produced [2]. For example Graham et al. demonstrated [3] the reaction (1) in low temperature matrices.

$$Cr(CO)_6 \xrightarrow[\text{Ar, 20 K}]{\text{UV}} Cr(CO)_5 + CO \tag{1}$$

The gaseous mixture may be sprayed on slowly and continuously over a period of time, or deposited in a series of short discrete pulses over a much shorter time [4]. The latter method is used whenever possible since this leads to less contamination of the matrix by vacuum residuals and probably better isolation. In contrast to small main group systems where matrix : reactant ratios (M/R) of 500 are typical, matrix isolation studies of transition metal carbonyl species usually employ ratios of 5000 or more. The larger size of these polyatomic transition metal systems (13 atoms for $Cr(CO)_6$ compared to 3 or 4 for a typical main group system studied by this method) requires the use of much higher ratios to minimise the formation of dimers and higher aggregates. Since lower carbonyl fragments are generated photolytically (eqns. 1,2) good

$$Ni(CO)_4 \xrightarrow[\text{Ar, 20 K}]{\text{Vac UV}} Ni(CO)_3 + CO \tag{2}$$

optical quality of the matrix is essential. This is especially true in the vacuum UV region (illustrated by Burdett's $Ni(CO)_3$ species [5] in (2)) where a cloudy or snowy matrix is an effective scatterer of the photolysing radiation.

(b) A stable molecule may be photolysed in a reactive matrix. Rest produced $Ni(CO)_3N_2(3)$ in this way [6]. Here use is made of the fact that the ini-

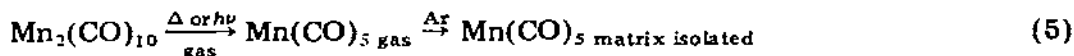$$Ni(CO)_4 \xrightarrow[\text{N}_2, 20 K]{\text{UV}} Ni(CO)_3N_2 + CO \tag{3}$$

tially produced $Ni(CO)_3$ reacts with the N_2 matrix itself.

(c) Two reactive species may be cocondensed from the gas phase to form a new species which is rapidly frozen and trapped as in the series of rhodium dinitrogen complexes (4) made by Ozin and Van der Voet [7].

$$Rh + N_2/Ar \rightarrow Rh(N_2)_4 \tag{4}$$

(d) A reactive species may be made in the gas phase and rapidly trapped in the matrix. In principle the $Mn(CO)_5$ species could be made either photochemically or thermally and rapidly condensed in the matrix with excess matrix gas (5).

$$Mn_2(CO)_{10} \xrightarrow[\text{gas}]{\Delta \text{ or } h\nu} Mn(CO)_{5 \text{ gas}} \xrightarrow{\text{Ar}} Mn(CO)_{5 \text{ matrix isolated}} \tag{5}$$

This is much more difficult than it appears and this sort of reaction has not yet been demonstrated in the carbonyl field. There are some other techniques which we will examine later with reference to specific problems. But let us

now examine in a little more detail the methods which have been almost
exclusively used for the study of transition metal carbonyls and related spe-
cies.

(ii) In situ photolytic generation

Figure 2 shows an example of an in situ photolytic generation [8—10]
of the unstable species $Fe(CO)_4$ and $Fe(CO)_3$. The IR spectra show how the
bands of $Fe(CO)_5$ decrease in intensity and those of $Fe(CO)_4$ grow in on UV
photolysis. A band also grows in due to free CO. On further photolysis bands
due to $Fe(CO)_3$ increase at the expense of both $Fe(CO)_4$ and $Fe(CO)_5$. Also
illustrated by these spectra is a complicating feature in many vibrational
studies of matrix isolated species. Some of the IR bands are split, sometimes
into as many as four components. The origin of these 'matrix splittings' is not
entirely clear, but each component probably represents an $Fe(CO)_4$ molecule
trapped in a slightly different environment in the matrix [11]. On extended
photolysis the UV/vis spectrum of the matrix shows [12] that Fe atoms are
present.

The sort of reactions that may occur photochemically in these low tempera-
ture matrices is substantially limited by the restrictions of the so-called cage
effect [13]. It is generally difficult to produce main group species by an in
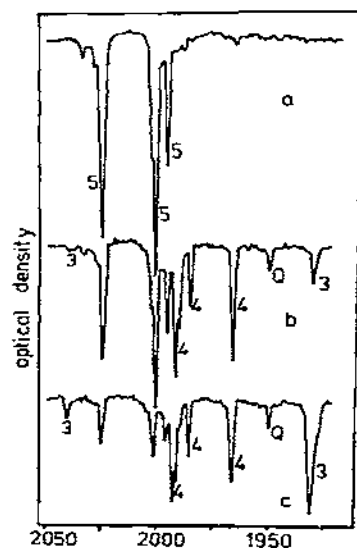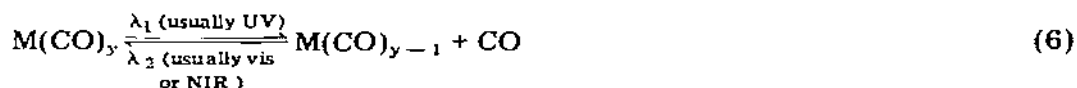

Fig. 2. Photolysis of $Fe(CO)_5$ in a CH_4 matrix at 20 K: (a) on deposition, note matrix
splittings on carbonyl bands of $Fe(CO)_5$ (labelled 5); (b) after 1 min, UV photolysis, new
bands due to $Fe(CO)_4$ and $Fe(CO)_3$ (labelled 4,3) appear. Also a weaker band due to
$Fe(CO)_4CH_4$ (labelled Q); (c) after 5 min, UV photolysis, bands of $Fe(CO)_5$ continue to
decrease in intensity as do bands due to $Fe(CO)_4$. Bands due to $Fe(CO)_3$ continue to
increase in intensity. (Adapted from ref. 10).

situ photolysis in inert matrices at 20 K by photoejection of a second row atom or larger because the atom is too large to squeeze readily through the lattice interstices and away from the newly formed unstable species. Thus the two fragments held together inside the matrix cage recombine to give the parent molecule back again. Similarly, although gas phase photolysis of cyanogen leads to liberal quantities of CN, photolysis of $(CN)_2$ in low temperature matrices is very inefficient [14]. The CN radical produced is probably too large to escape from the matrix cage and readily recombines with its partner to regenerate the parent $(CN)_2$. The CN radical is certainly of a similar size to the CO molecule, and this observation leads us to ask a very obvious question. If diffusion of the CO away from the photolysis site is an unlikely event, how is it possible to generate carbonyl fragments by photolysis of a parent carbonyl trapped in the matrix? From solution flash photolysis studies it is well known that these unsaturated carbonyls react rapidly with CO, phosphines etc. The answer to this question lies in a series of detailed experiments over the past few years to which we turn in more detail later. In brief, however, the photoproduced molecule undergoes an intramolecular rearrangement so as to lie in a position from which rapid CO recombination will not occur. 1 shows the scheme postulated for $Cr(CO)_5$. On going from left to right the excited
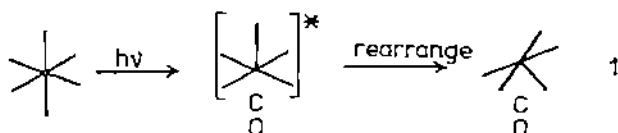
pentacarbonyl fragment rearranges and is frozen in a spatial orientation such that there is a matrix molecule and not a CO molecule in the sixth coordination site of the metal. On visible photolysis of the pentacarbonyl, however, a photochemical rearrangement is possible to reestablish the original spatial description of the ligands relative to the photoejected CO such that thermal recombination is possible. Thus these trapped carbonyl species often clearly show photochromic behavior (eqn. 6). Sometimes the reverse step is so facile that a filtered Hg arc is needed for efficient production of the fragment and the visible and near IR radiation must be removed from the IR spectrometer beam used for product detection and characterization (with a germanium filter). This photochromic behavior means that laser Raman spectroscopy cannot

$$M(CO)_y \underset{\lambda_2 \text{ (usually vis or NIR)}}{\overset{\lambda_1 \text{ (usually UV)}}{\rightleftharpoons}} M(CO)_{y-1} + CO \tag{6}$$

usually be used for product characterization. The light of the laser probe itself reverses [85] the forward photolysis step. (Raman spectroscopy is however a useful tool in other situations where the new species has been made by some other method e.g. atom cocondensation and the technique has been extensively used by the Toronto group.)

The implication in 1 that the carbonyl fragment and CO share the same matrix cage is supported by the observation of splittings which appear in the IR spectrum of the fragment due to its perturbation by CO. However, on extended photolysis of $Fe(CO)_5$ for example, Poliakoff and Turner showed that new IR bands grow in close to these split ones which arise from carbonyl fragments where the CO has been ejected from the matrix cage [9]. This low yield process (cf. the cyanogen photolysis above) becomes significant after long photolysis times and produces a carbonyl fragment which is stable to the reversing radiation of (6). This is called the 'irreversible' material. (The species which is readily reversed to parent is called 'reversible'.) In the region associated with free CO two bands are also present on long photolysis. The one which grows in last is in the same place as that found for matrix isolated CO starting from a gaseous mixture of CO and e.g. Ar. It corresponds to free, essentially unperturbed (by fragment) CO. The other band is associated with the reversible fragment and represents those CO molecules which are contained in the same matrix cage as the carbonyl fragment. On visible irradiation the intensity of this band decreases due to recombination of CO with fragment to give parent. Similar but more complex behavior occurs with other carbonyls studied in this way [15,16]. These splittings occur in addition to the matrix site effects we noted above.

(iii) Metal atom reactions

A solid lump of metal is often very unreactive towards gaseous CO or N_2. The opposite is true when the metal is in the form of metal atoms, dimers or small metal clusters [17]. Cocondensation of metal vapor with either pure or diluted matrices of ligand $L(=CO, N_2, O_2, C_2H_4, C_2H_2)$ leads to matrix isolated $M_x L_y$ species [18]. By using larger metal atom fluxes and working at 77 K it is possible to produce macroscopic (gram) quantities of new material when the matrix (usually a hydrocarbon) is warmed to room temperature [19—22]. This has led to the synthesis, mainly by the groups of Timms, Klabunde, Green and the late Koerner von Gustorf, of new molecules which are difficult to prepare in more conventional ways. Our review will not be concerned with this aspect of metal vapor chemistry but will concentrate on the microscopic aspects in very low temperature matrices [23]. The slow spray-on technique has to be used in these experiments and several early studies did not anticipate the rapid reaction of the metal atoms with the impurities in the vacuum system [24,25]. In order to ensure that a beam of monatomic vapor is produced the majority of recent work has used double ovens to vaporise the metal and dissociate polymers. A very useful way of monitoring the amount of metal emanating from the source is to use a quartz crystal microbalance [26]. Even when it is certain that a beam of monatomic metal vapor is being condensed with CO or N_2 and matrix gas, new species containing more than one metal atom are often found. For example in the cocondensation of Mn atoms and CO/Ar mixtures, by far the most prominent product is $Mn_2(CO)_{10}$ [27]. The reason for this is diffusion of the metal atoms in the liquid-like surface

layer of the matrix before it freezes solid. A kinetic analysis of the problem leads to a polymer concentration dependence of the form of eqn. 7 where M_n

$$M_n \propto M_1 M_0^{n-1} \qquad\qquad (7)$$

is the concentration of the $n$mer and M_0 the total concentration of metal.

Thus in order to avoid the formation of polynuclears, experiments must be done at high dilution. This sometimes creates problems since at very low metal atom concentrations the small number of reactive metal atoms are quickly used up as "getters' in the vacuum system. The electronic spectra of a variety of metal atoms and $n$mers have been studied in matrices [28—32].

The tremendous advantage of the atom cocondensation method is, however that the cage restrictions of the photochemical approach do not apply and new species may be made without relying on the availability of a stable precursor. For example $Cu(CO)_3$ [33] and $Al(CO)_2$ [34] have been made in low temperature matrices by cocondensation methods even though there are no stable binary copper or aluminum carbonyls. Binary dinitrogen complexes have been made exclusively by this technique since no stable binary dinitrogen species are available.

$$M + yN_2 \rightarrow M(N_2)_y \qquad\qquad (8)$$

(There is some limited evidence [35] to suggest that extended photolysis of $Cr(CO)_6$ in pure N_2 matrices leads to $Cr(N_2)_6$ [36].) The majority of recent work in this field has come from the laboratories of Professor G.A. Ozin at Toronto.

Figure 3 shows the results of the first matrix synthesis by DeKock [37] of a transition metal carbonyl by this method. Nickel atoms were cocondensed with an Ar/CO mixture (200 : 1) at 4 K [37]. The top spectrum shows a strong absorption at 1996 cm^{-1} due to NiCO, and intense band due to unreacted CO. On warming the matrix bands grow in due to $Ni(CO)_2$, $Ni(CO)_3$ and finally $Ni(CO)_4$. As the temperature is raised NiCO is consumed to form higher carbonyls. Eventually the temperature is raised to a point so that diffusion may occur in the matrix and polymeric species and $Ni(CO)_4$ aggregates may be formed. This gives rise to the broad featureless absorption at the bottom of Fig. 3. In addition to the bands assigned to mononuclear carbonyls, another band at 2035 cm^{-1} appears on warming. This is most likely due to a $Ni_2(CO)_x$ species although no detailed structural data are available to confirm this assignment. The atom cocondensation method is therefore the exact opposite of the photochemical one described above — adding on CO ligands to the naked metal atom rather than stripping them off a coordinatively saturated one. If the major disadvantage of the photolysis method is the cage effect and the availability of a stable precursor, then the disadvantage of the metal vapor method is the production of bi- or polynuclear species (if one wants to produce single metal atom containing complexes) and, as we will see later, of identifying them when they are formed. There is also the added complication that often several species will be present in the matrix at once (see our discussion
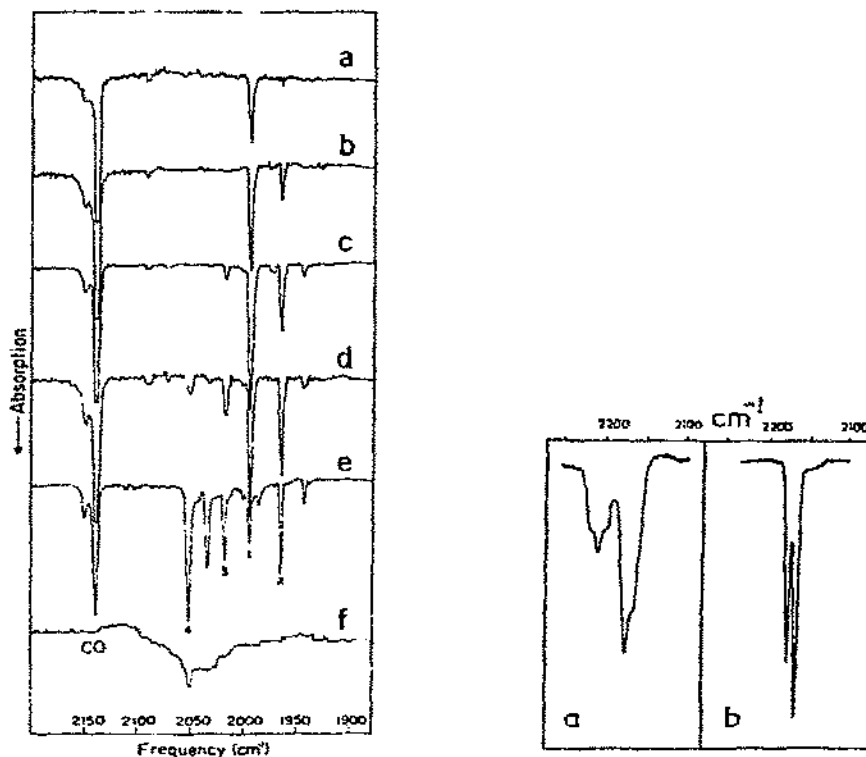
Fig. 3. Matrix synthesis of Ni(CO)$_y$ by cocondensation of Ni atoms with Ar/CO mixtures: (a) after deposition of 4.2 K a single band due to NiCO; (b)—(e) on annealing to 20 K bands due to Ni(CO)$_{1-4}$ grow in (labelled 1—4). On raising the temperature to 35 K (f) aggregation occurs and isolation is lost. (The extra bands growing in on annealing and not labelled in (e) are almost certainly due to Ni$_2$(CO)$_y$ species. Reproduced by permission from Ref. 37.

Fig. 4. Cocondensation of Ni atoms with N$_2$ at 20 K: (a) fast metal atom evaporation leads to two features: the higher frequency absorption is due to Ni$_{cl}$N$_2$ and the lower frequency one due to poorly isolated Ni(N$_2$)$_4$; (b) slow metal atom evaporation gives only bands due to the molecular complex.

on the Cr(CO)$_3$ controversy below) which makes the task of unravelling their spectra and characterizing them via isotopic substitution rather complex.

Formation of metal atom clusters, however, is not always a disadvantage. One field which has not been explored extensively but which is receiving increasing attention, especially for the case of L=ethylene, is the synthesis and structural characterization of M$_x$L$_y$ species with L = CO, N$_2$ where $x > 1$. In general, if x is large and equivalent to a cluster (cl) of atoms, then the species produced, M$_{cl}$L$_y$ or M$_{cl}$L may well be a good model for the chemisorption of L on the metal M. Figure 4 shows the IR spectrum of the Ni(N$_2$)$_4$ molecule made by Burdett and Turner via a low Ni atom flux condensed with pure N$_2$ [38,39]. (In refs. 38, 39 these bands were incorrectly assigned to a lower

dinitrogen complex.) On increasing the rate of metal atom evaporation, new bands grow in at 2188 cm^{-1} and 2196 cm^{-1} which may be due to $Ni_x(N_2)_y$ species with x = 2, 3. To higher frequency at 2206 cm^{-1} a band grows in with higher Ni atom concentrations which is assigned to N_2 chemisorbed in a Ni atom cluster. Conventional IR studies of chemisorbed N_2 on a clean Ni surface give a value of 2202 cm^{-1} for the ν(NN) frequency [40]. The matrix medium provides a way of observing the IR spectrum of chemisorbed ligands which might be difficult to study conventionally. For example, evaporation of Cu metal into an N_2 matrix leads to an infra-red absorption at 2272 cm^{-1}, surely too high for a molecular species and almost certainly due to $Cu_{cl}N_2$ [39]. No conventional IR measurements of N_2 chemisorbed on Cu have been reported. (The relatively small frequency shift from gaseous N_2 (2331 cm^{-1}) of ν(NN) possibly indicates a weak bond between metal and N_2, which may mean that conventional studies would be difficult.) One of the advantages of this method is that the metal surface is produced under 'clean' conditions. The cluster is surrounded by Ar or other inert material compared to the surface layer of grease or water which may contaminate more conventional systems.

The metal atom cocondensation method has been used to produce new species with a variety of ligands. In addition to CO and N_2, ethylene, acetylene and O_2 have also been used by Ozin and co-workers to produce a considerable range of new species. Recently evaporation of Ni atoms into C_2H_4/Ar matrices in a controlled fashion has led to the formation [41] of $Ni_2(C_2H_4)$ with very similar UV/vis and IR spectra to $Ni(C_2H_4)$. The importance of such species in understanding the role of the metal in heterogeneous catalytic process is clear and we shall discuss below some aspects of the problem in the light of recent results.

(iv) Studies using low temperature glasses

One way to study photochemical reactions of a carbonyl or other species without the necessity of cryogenic equipment and high vacua is to use glassy materials as 'matrices' at higher temperatures, usually 77 K. A solution of a stable precursor may be made in a mixture of, say, isopentane and methylcyclohexane and rapidly frozen to a glass at liquid nitrogen temperatures between two sapphire windows in a suitable cold cell. Rapid freezing is required otherwise the solute simply crystallises from solution. Once the glass has been successfully produced, however, the photochemical reactions of the trapped species may be followed as in the very low temperature method [42—45]. The technique has its limitations however. Firstly in these media the IR bands are not usually very sharp which reduces their value for structural characterization since overlapping features may easily be missed. Secondly, there is evidence that these glassy materials are not 'inert' matrices and may interact in a significant way with the carbonyl fragment. In addition there is evidence [46] that impurities such as water preferentially associate with the dissolved carbonyl and are therefore ideally placed to interact with the fragment when it is produced. There is however some evidence that the cage

effect in these systems is a less serious problem than in matrices at much lower temperatures probably because of a less closely packed arrangement. One of the attractions of the approach is that the matrix may be melted and the products of reaction of the photochemically produced species detected in solution. As we noted above hydrocarbon matrices are often used in macroscopic metal vapor chemistry [47].

A method related to the glass technique is that of suspending the stable precursor molecule in a polymer and studying photochemical reactions in the same way. For example the photolysis reaction (1) was studied by dissolving Cr(CO)$_6$ in methyl methacrylate, initiating the polymerisation and later studying the photochemistry in the 'room temperature glass' [48]. Alternatively Cr(CO)$_6$ may be supported in polyethylene film or PVC film and the system cooled to cryogenic temperatures where the photochemistry may be studied. First the carbonyl is dissolved in a suitable solvent in which the film is immersed. The solvent is then judiciously removed under vacuum as the temperature is lowered to leave behind suspended carbonyl. Obviously if the solvent is pulled off too vigorously at too high a temperature the carbonyl is removed from the film as well. The method usually leads to a small amount of solvent left behind in the film. These polymeric materials at low temperatures do seem to be rather cavernous on a microscopic scale and diffusion of photo-ejected CO away from the photolysis site occurs relatively easily. The IR stretching bands of the carbonyl species are usually quite broad in these polymeric media.

Although studies in these higher temperature matrices are interesting, we shall restrict the scope of the review to studies in the low temperature matrix environment.

C. STRUCTURAL CHARACTERIZATION OF THE CARBONYL FRAGMENT

(i) Use of isotopes

As mentioned above structural characterization of the new species may often be achieved elegantly by the use of IR spectroscopy. This is a much more powerful tool in the realm of carbonyl chemistry for such a purpose than in main group systems or non-carbonyls as we see later in this section [49]. Firstly by the use of naturally occurring CO in the atom method or of an unenriched carbonyl in the photolysis method, the new carbonyl molecule will be almost exclusively $M(^{12}C^{16}O)_y$, (^{13}CO is present as $\sim 1\%$ in naturally occurring CO) and, at most, y absorptions will be observed in the carbonyl stretching region. Allowing for the fact that some bands may be weak and unobserved, or forbidden on group theoretical grounds and that degeneracies may occur, the number of new IR bands is not a reliable guide on its own to the stoichiometry or structure of the new carbonyl species. Additional information as to the nature of the new molecule may be obtained by recording the spectrum of the new carbonyl enriched with one of the readily available isotopes $^{13}C^{16}O$, $^{12}C^{18}O$ or the double isotope $^{13}C^{18}O$. In the atom method a

suitable gas phase mixture of $Ar/^{12}C^{16}O /^{P}C^{q}O$ must be made. In the photolysis method the enrichment process involves reaction of the stable precursor with labelled CO to produce a statistical mixture of the $M(^{12}C^{16}O)_{y-z}(^{P}C^{q}O)_{z}$ parent. This usually involves a photochemical reaction in the gas phase or solution between $M(^{12}C^{16}O)_{y}$ and the isotopic CO using the method of Crichton and Rest [50]. After separation of the carbonyl and CO the matrix isolation experiment proceeds in the usual way. The number and frequencies of the new IR bands observed for the $M(CO)_{y-1}$ and $M(CO)_{y-2}$ species due to such labelling are often sufficient to pin down the number of carbonyl groups in the molecule and sometimes its qualitative structure [51]. Similar isotopic studies may be employed with other ligands (N_2, O_2, C_2H_4 etc.). We will focus here on the results obtained with carbonyls since it is with the CO ligand that the bulk of the spectroscopic sophistication has been achieved.

Figure 5 shows the results of isotopic substitution in $Fe(CO)_3$, a pyramidal molecule [10]. The parent and totally substituted species are of C_{3v} symmetry and the carbonyl stretching vibrations transform as $a_1 + e$. The a_1 vibrations of the two species are found at 2039.8 cm^{-1} and about 1994 cm^{-1}. The two partially substituted species are of C_s symmetry and the carbonyl vibrations
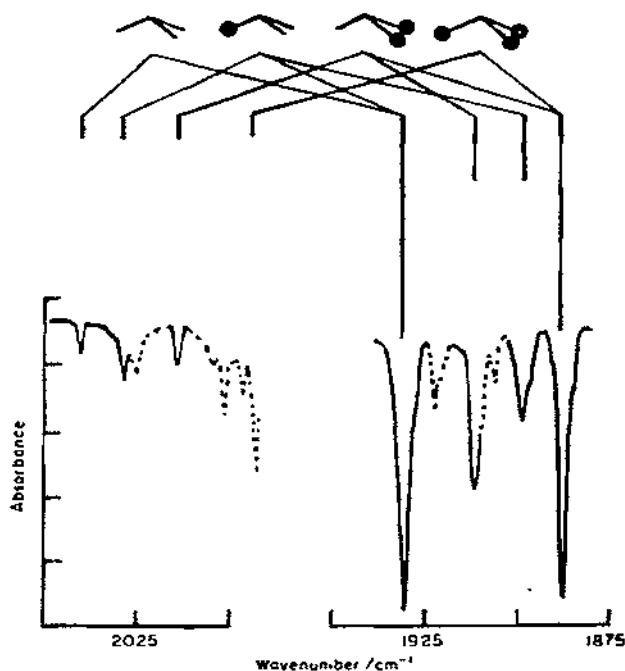

Fig. 5. Observed and calculated (bond angle 109.4°) IR spectra for a mixture of $Fe(^{12}CO)_{3-z}(^{13}CO)_z$ (z = 0—3) in a CH$_4$ matrix at 20 K. The bands with broken lines are due to $Fe(CO)_{4,5}$. The black circles represent ^{13}CO molecules. (Adapted from ref. 49).

transform as $2a' + a''$ i.e. in the lower symmetry $a_1 \to a'$, $e \to a' + a''$. The a'' vibration occurs at the same frequency as the e vibration in the relevant C_{3v} parent as shown in 2. The parentage of the IR bands in the $Fe(CO)_3$ spectrum

$* = {}^{13}CO$ $\underline{2}$
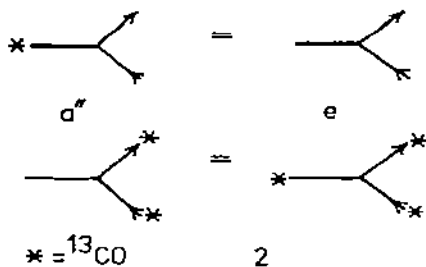
is shown in Fig. 5. The isotopic splitting pattern is then totally consistent in qualitative terms with a pyramidal C_{3v} molecule.

In these isotopic studies care needs to be exercised that the matrix actually contains what you think it does. Thus for example in one heated debate Kundig and Ozin published an isotopic spectrum of $Cr(CO)_5$ made by the atom method which was claimed to fit the D_{3h} model [52]. This was in stark contradiction to the C_{4v} structure claimed by Perutz and Turner from analysis of the photolytically produced system [53]. The discrepancy was finally resolved in favor of the C_{4v} model, the isotopic spectrum of the D_{3h} form being a composite of parts of the isotopic spectra of $Cr(CO)_6$, $Cr(CO)_5$ and $Cr(CO)_4$ [54]. The structures predicted for $Cr(CO)_5$ as we will see later should be C_{4v} for the lowest singlet and D_{3h} for the lowest triplet. It is clear that further effort will be made in this field to find conditions under which a D_{3h} molecule is stable.

(ii) The frequency factored force field (F^4)

A more challenging test of the isotopic assignment is a numerical fit of the CO stretching frequencies with a vibrational force field.

The general vibrational problem is described by eqns. 9 and 10.

$$GFL = \lambda L \tag{9}$$

$$|GF - \lambda E| = 0 \tag{10}$$

G is the inverse kinetic energy matrix and contains terms involving the masses of the atoms in the molecule and their arrangement in space, via the geometrical configuration parameters bond angles and bond lengths. F is a matrix containing the force constants representing the stretching, bending and other deformations of the molecular frame. L is the eigenvector matrix and relates the normal (N) and internal symmetry (Q) modes (eqn. 11). The general solution of the vibrational problem with $3n - 6$ vibrations for an n-atomic non-

$$S = LQ \tag{11}$$

linear molecule and up to $\bar{n}(\bar{n}/2 + 1)$ force constants ($\bar{n}$ is the number of vibra-

tions of the isotopically pure molecule) is a complex task. It has been achieved for various stable, high symmetry carbonyls (e.g. $Cr(CO)_6$ [55], $Fe(CO)_5$ [56], $Ni(CO)_4$ [57] and $Mn(CO)_5Br$ [58]) and the parameters of a general quadratic valence force field (GQVFF) obtained. It is impossible to achieve for the newly made carbonyl fragment where only very scanty data are usually available for the low frequency region where the modes involving the internal coordinates of MC stretching and MCO deformations occur. In addition the number of GQVFF constants may well be large since often the new species is of low symmetry. However it has long been recognised that the carbonyl vibrations alone may be treated as if they were completely decoupled from the rest of the molecule [59—62]. In this high-frequency approximation the force field is frequency factored (i.e. only CO stretching and CO, CO stretch—stretch interaction force constants appear) and the carbonyl vibrations at between 1800 and 2100 cm^{-1} separated from the other motions of the molecule occurring at 600 cm^{-1} and below. One particular version of the F^A, the Cotton—Kraihanzel [59] force field involves an extra assumption originally suggested by Jones [63] about the relative sizes of the interaction constants which we will not use.

Let us see what the approximations are in this sort of approach [64] by considering the vibrations contained in one symmetry representation (Γ) of the molecular point group of a binary carbonyl. We consider the case where one "CO stretching", one "MC stretching" and one deformation of the molecule are contained within this representation. A mixing of the internal symmetry modes ($S = R_{CO}, R_{MC}, R_\delta$) occurs to give three normal modes which in principle may be observed spectroscopically. From eqn. 11 for these three modes, eqn. 12 is derived for Q_{1-3}. Q_1 will be observed in the "carbonyl stretching" region and $Q_{2,3}$ at low frequency. The largest elements of L are the diagonal ones. From eqn. 9 the 'carbonyl stretching frequency' ν_{CO} is given by eqn. 13

$$R_{CO} = Q_1 L_{11} + Q_2 L_{21} + Q_3 L_{31}$$

$$R_{MC} = Q_1 L_{12} + Q_2 L_{22} + Q_3 L_{32} \tag{12}$$

$$R_\delta = Q_1 L_{13} + Q_2 L_{23} + Q_3 L_{33}$$

where $\lambda = 4\pi^2 c^2 \nu^2$. Now the bending vibrations are expected to contribute

$$\lambda_{CO} L_{11} = (GF)_{11} L_{11} + (GF)_{12} L_{21} + (GF)_{13} L_{31} \tag{13}$$

minimally to the highest frequency ($\nu(CO)$) vibration. Since these MCO units are linear, vibrational coupling of a particular CO stretch to the bending motion of the same unit is forbidden by symmetry. Thus any coupling will be of long range and therefore small. So we put $L_{31} = 0$ and get eqn. 14. The ratio L_{21}/L_{11} may be evaluated by making use of the identity $L\tilde{L} = G$ which leads

$$\lambda_{CO} = (GF)_{11} + (GF)_{12} \frac{L_{21}}{L_{11}} \tag{14}$$

initially to the relationship (15). Simplification of this expression may be

achieved by the adoption of a result from GQVFF studies on carbonyls [65].

$$\frac{G_{12}}{G_{11}} = \frac{L_{11}L_{21} + L_{12}L_{22}}{L_{11}^2 + L_{12}^2} \tag{15}$$

There seems to be very little carbonyl stretching involved in any of the low frequency modes. This puts $L_{12} = 0$ and with μ_i representing the inverse mass of atom i, gives (16) ready for substitution into (14).

$$\frac{L_{21}}{L_{11}} = \frac{G_{12}}{G_{11}} = \frac{-\mu_c}{\mu_c + \mu_0} = -x \tag{16}$$

After evaluation of the elements of GF this leads to a particularly simple expression for the carbonyl stretching frequency (17). The $F_{ij}(\Gamma)$ are the sym-

$$\lambda_{CO} = (\mu_c + \mu_0)[F_{11}(\Gamma) - 2\,xF_{12}(\Gamma) + x^2F_{22}(\Gamma)] \tag{17}$$

metry combinations of force constants describing the internal modes R_{MC}, R_{CO}. For the σ_u^+ stretching vibrations of a linear $(D_{\infty h})$ M(CO)$_2$ unit for example, $F_{11}(\sigma_u^+) = f_{CO} - f_{CO,CO'}$, $F_{12}(\sigma_u^+) = f_{CO,MC} - f_{CO,MC'}$, $F_{22}(\sigma_u^+) f_{MC} - f_{MC,MC'}$ where the primes refer to interaction with a different MCO unit. The f's are the valence stretching and stretch—stretch interaction force constants of the GQVFF. Equation 17 is to be compared with the frequency factored approach of eqn. 18. $K(\Gamma)$ is the symmetry adapted set of carbonyl stretching force

$$\lambda_{CO} = (\mu_c + \mu_0)K(\Gamma) \tag{18}$$

constants alone since all others are ignored. The G matrix element is simply the inverse reduced mass, $\mu_c + \mu_0$, of the carbonyl group. For the $D_{\infty h}$ M(CO)$_2$ molecule $K(\sigma_u^+) = k_{CO} - k_{CO,CO'}$. For the harmonic oscillator the frequency factored force constants (k's) are just weighted sums of the GQVFF constants (f's), but dominated from eqn. 17 by the leading term f_{CO} which is much larger than any competitor, f_{MC} or $f_{MC,CO}$. Solution of the F^a problem of eqn. 19 where $\mu_{CO} = \mu_c + \mu_0$ then gives a set of F^a constants k_{CO}'s and $k_{CO,CO'}$ which reproduce well the observed vibrational frequencies of the molecule as

$$|\mu_{CO}K - \lambda_{CO}E| = 0 \tag{19}$$

we will see below.

One point that is clear from eqn. 17 is that the value of $K(\Gamma)$ and hence k_{CO} is a function of the isotope used in the calculation via the terms in x. Alternatively the isotope shift in a $\nu(CO)$ vibration on substitution will not be given exactly by the implication of eqn. 18 as

$$\lambda'_{CO}/\lambda_{CO} = \mu'_{CO}/\mu_{CO} = R^2 \tag{20}$$

where the primes refer to the heavier isotope.

One other factor which will affect the isotope shift is the effect of anharmonicity. Since the anharmonic correction depends upon frequency, a different correction will apply to the harmonic frequency of parent and isotopically substituted molecule. The isotope shifts for the t_{1u} carbonyl stretching mode of Cr(CO)$_6$ are given in Table 1. As can be seen the observed shift for the $^{13}C^{16}O$ isotope is given quite well by the F^a but the others are not. In-

TABLE 1

Breakdown of the errors involved in the F^4 method for the t_{1u} mode of $Cr(^{12}C^qO)_6$ isolated in a CH_4 matrix at 20 K [c]

Isotope	$^{13}C^{16}O$	$^{12}C^{18}O$	$^{13}C^{18}O$
ν(obs)	1941.7 cm^{-1}	1939.4 cm^{-1}	1894.0 cm^{-1}
$\nu(F^4)$ [a]	1941.1	1937.4	1892.1
Error (observed)	0.6	2.0	1.9
x factor correction (eqn. 17)	−0.3	0.6	0.2
Anharmonicity	0.9	1.0	1.9
Error (calculated)	0.6	1.6	2.1
Standard deviation [b]	0.31	0.67	0.61
Maximum error [b]	0.9	1.6	1.6
Number of observed bands [b]	19	15	20

[a] $\nu(t_{1u})$ for $Cr(^{12}C^{16}O)_6$ is at 1985.4 cm^{-1}. [b] From a least squares refinement using the frequencies of the $Cr(^{12}C^{16}O)_z$ $(^{12}C^qO)_{6-z}$ molecules. [c] Adapted from ref. 64.

spection of the middle section of Table 1 tells us why. For the $^{13}C^{16}O$ substitution the anharmonic correction and x factor corrections from eqn. 17 nearly cancel, for the other two isotopes they add together. In the last row of Table 1 are the standard deviations for observed—calculated frequencies using the F^4 and each of the isotopic substitutions. Clearly the $^{13}C^{16}O$ substitution is best for the reason we have pinpointed here. The best vibrational studies using the F^4 method will therefore be those with $^{13}C^{16}O$ substitution. The figure for the standard deviation in Table 1 for such a substitution, 0.31 cm^{-1}, is very good indeed and considerably smaller than usually found in force field studies [66]. The error may be reduced further — sometimes as low as 0.2 cm^{-1} — if an additional parameter is included in the force field problem. This is the 'effective' reduced mass ratio (eqn. 21) introduced by Bor [67].

$$\nu_i'/\nu_i = R_{eff} = (\mu'_{eff}/\mu_{12,16})^{1/2} \tag{21}$$

R/R_{eff} (eqns. 20,21) is very close to unity. This absorbs further the remaining errors in the F^4.

In practice, therefore, in order to determine the geometry of a molecule qualitatively, the carbonyl IR spectrum of the parent $M(CO)_y$ and isotopic variants $M(CO)_{y-z}(C'O')_z$ must be accurately measured. The vibrational force constants and the R parameter of eqn. 21 are refined in a least-squares way with these observed frequencies for a particular assumed molecular geometry. A series of molecular geometries may be tried, C_{3v} or D_{2d} for example for an $M(CO)_4$ molecule. The one which gives the best agreement between observed and calculated frequencies is probably the correct geometry. Figure 6 shows the IR spectrum of $Cr(CO)_5$ recorded by Perutz and Turner via photolysis

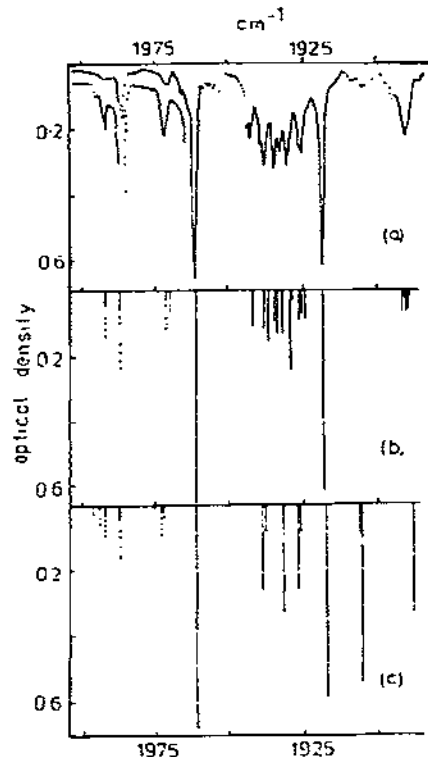Fig. 6. (a) Observed spectrum of $Cr(^{12}CO)_{5-z}(^{13}CO)_z$ molecules in a CH_4 matrix at 20 K. (b) Calculated 'stick' spectrum for a C_{4v} model. (c) Calculated 'stick' spectrum for a D_{3h} model. From ref. 53 with permission.

[53] of a scrambled $Cr(^{12}C^{16}O)_{6-z}(^{13}C^{16}O)_z$ sample. Above are stick spectra corresponding to two possible molecular geometries, the trigonal bipyramid (D_{3h}) and the square based pyramid (C_{4v}). It is clear that completely different spectra result, and the better fit is undoubtedly achieved for the C_{4v} geometry. Other systems are sometimes not quite as clearcut. For example the d^9 system $Fe(CO)_4^-$ has been shown to have a C_{3v} structure, but the difference in standard errors between C_{3v} and D_{2d} models was significant but not huge; C_{3v} 0.62 cm^{-1}, D_{2d} 1.7 cm^{-1} [68].

For N_2 as a ligand the situation is rather different. The value of x in eqn. 17 is equal to 0.5 for both $^{14}N_2$ and $^{15}N_2$ isotopes, so the F^a approximation holds exactly for the *harmonic* oscillator. Thus the observed deviations from the force field are due to anharmonic corrections alone. (In principle we could determine the anharmonicities from the isotope shift but they are subject to large errors.) In general larger errors are observed experimentally in binary N_2 complexes compared to $^{13}C^{16}O$ substitutions in binary carbonyls.

(iii) Infra-red intensities

One additional piece of information from the infra-red spectrum which may be used to quantify the structure determination is the use of relative intensity measurements [51,69,70—76]. This is a field in which several people have made contributions, mainly in the application of the method to determination of the geometry of stable molecules from solution spectra. For example, calculation of the intensity pattern of the $M(CO)_5$ species of the previous section as a function of geometry gave added reasons for rejecting the tbp geometry. A much better intensity and frequency fit is obtained for the spy structure. The intensity of an infra-red absorption is proportional to $(d\mu/dQ)_0^2$, the square of the dipole moment derivative on vibration (μ is not to be confused with the reciprocal of the reduced mass of the CO group μ_{CO}). Since the normal modes are related to the symmetry modes by eqn. 11 and these symmetry modes to the internal modes R by eqn. 22, where U may be simply determined by group theory,
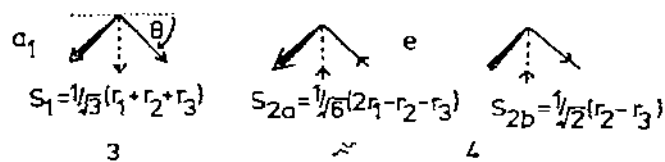
$$S = UR \qquad (22)$$

we can write for the intensity of the ith normal mode

$$I_i \alpha \left[\sum_k \sum_j U_{jk} L_{ij} \frac{d\mu}{dR_k} \right]^2 \qquad (23)$$

Thus the intensity depends on the directions in space in which the dipole moment changes occur on stretching individual (R_k) CO bonds. We assume that this occurs parallel to the MCO axis although there is no definitive evidence to support this claim. Brown and Darensbourg [74,75] have developed another method, slightly different to the one we use here in which the dipole moment change of a particular MCO group depends upon the symmetry species of the vibration. The present author believes this to be an incorrect approach (see ref. 49 for a discussion). One problem associated with this method is that some of the failures associated with the IR-intensity method, which we discuss later, are hidden in an extra parameter (ρ).

The use of eqn. 23 is best illustrated by two examples, the determination of the bond angles in pyramidal $Fe(CO)_3$ and square pyramidal $Cr(CO)_5$. For $Fe(CO)_3$ [10] the totally symmetric (a_1) and degenerate asymmetric (e) carbonyl stretching vibrations are shown in 3 and 4, with their description in

$$a_1 \qquad \qquad e$$
$$S_1 = \tfrac{1}{\sqrt{3}}(r_1 + r_2 + r_3) \qquad S_{2a} = \tfrac{1}{\sqrt{6}}(2r_1 - r_2 - r_3) \qquad S_{2b} = \tfrac{1}{\sqrt{2}}(r_2 - r_3)$$
$$\underline{3} \qquad \qquad \underline{4}$$

terms of the internal modes r_{1-3} representing stretching of each of the 3 CO bonds. Since only one carbonyl stretching vibration is contained in each symmetry representation $L_{12} = 0$ and $L_{11} = L_{22} = \mu_{CO}^{1/2}$. This latter result follows simply from the identity $LL = G$ applied to the F^4. Substitution into eqn. 22

leads to eqns. 24 and 25, for the a_1 mode and both components of the e mode.

$$I(a_1) \propto [3^{-1/2} \mu_{CO}^{1/2} \; 3 \sin \theta \mu']^2 = 3 \, \mu_{CO} \mu'^2 \sin^2\theta \tag{24}$$

$$I(e) \propto [2^{-1/2} \mu_{CO}^{1/2} \; 3^{1/2} \cos \theta \mu']^2 + [6^{-1/2} \mu_{CO}^{1/2} \; 3 \cos \theta \mu']^2 = 3 \, \mu_{CO} \mu'^2 \cos^2\theta \tag{25}$$

where $\mu' = (\partial\mu/\partial R)_0$. Measurement of the relative intensity of a_1 and e modes for $Fe(CO)_3$ leads to ready determination of the bond angle θ (eqn. 26).

$$\frac{I(a_1)}{I(e)} = \tan^2\theta \tag{26}$$

This particular result is accessible without the need to know the details of the vibrational force field. For the $Cr(CO)_5$ unit however [53] in the IR there are three symmetry modes $2a_1 + e$ (27) two of which will mix together (5).
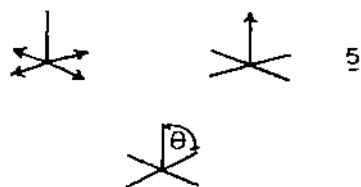
$$
\begin{aligned}
S_1 &= r_1 \\
S_2 &= \tfrac{1}{2}(r_2 + r_3 + r_4 + r_5) \\
S_{3a} &= 2^{-1/2}(r_3 - r_5) \\
S_{3b} &= 2^{-1/2}(r_2 - r_4)
\end{aligned}
\tag{27}
$$

S_1 and S_2 are both of the same symmetry (a_1) and mix (28) to give two a_1 normal modes Q_1, Q_2 where in this two dimensional problem $L_{21} = L_{12}$, $L_{11} = L_{22}$. These are observed at 2087.8 cm^{-1} and 1931.8 cm^{-1} for $Cr(^{12}C^{16}O)_5$ in solid Ar. We will refer to these as the high and low frequency a_1 vibrations respec-

$$
\begin{aligned}
S_1 &= Q_1 L_{11} + Q_2 L_{21} \\
S_2 &= Q_1 L_{12} + Q_2 L_{22}
\end{aligned}
\tag{28}
$$

tively. The e mode $Q_3(=S_3 L_{33}^{-1})$ is found at 1960.8 cm^{-1}. Substitution into eqn. (23) gives three equations for the IR intensities (eqns. 29–31) where μ'_a, μ'_b are the bond dipole moment derivatives of the chemically different MCO groups in the molecule, axial and basal.

$$I(a_1,\text{hi}) = \mu_{CO}(\mu'_a L_{11} - 2\mu'_b L_{12} \cos \theta)^2 \tag{29}$$

$$I(a_1,\text{lo}) = \mu_{CO}(\mu'_a L_{12} + 2\mu'_b L_{11} \cos \theta)^2 \tag{30}$$

$$I(e) = 4\mu_{CO}\mu'^2_b \sin^2\theta \tag{31}$$

The eigenvectors (L_{ij}) are determined from the vibrational force field for the

molecule using the F^4 method. Measurement of the relative intensities of all three bands ($R_1 = I(a_1, \text{hi})/I(a_1, \text{lo})$, $R_2 = I(e)/I(a_1, \text{lo})$) gives two pieces of data, sufficient to determine the bond angle θ and the ratio μ'_a/μ'_b (eqns. 32 and 33). The arithmetic manipulation used to derive these two values involves a square root with the consequent sign ambiguity. Physically it reduces to whether the

$$\theta = \tan^{-1}[R_2^{1/2}/(L_{11}R_1^{1/2} - L_{12})] \tag{32}$$

$$\mu'_a/\mu'_b = 2 \sin \theta (L_{11} + R_1^{1/2} \cdot L_{12})/R_2^{1/2} \tag{33}$$

two modes S_1 and S_2 are mixed in-phase in Q_1 or out-of-phase. The only way to find out which solution is correct is to calculate the intensities of all the bands in the isotopic spectrum for both sets of θ, μ' values and to compare with experiment. The high frequency region of the spectrum is particularly sensitive to this test. In the case of $Cr(CO)_5$ the in-phase solution is the correct one [53]. For $Mo(CO)_4$, however, the out-of-phase solution is the correct one [77]. A theoretical study exists which predicts the correct phase as a function of molecular geometry [78].

The accuracy of the bond angle determination depends upon three factors, over two of which we have some sort of control. (a) The relative intensities of the bands involved. The matrix method usually gives sharp bands which can often be measured quite accurately. Inaccuracies start to arise in spectra where the bands are split. (b) The accuracy with which the normal modes are described in terms of the symmetry and internal modes, when there are two or more CO stretching bands of the same symmetry. This depends on the accuracy of the force field. In general, the smaller the standard deviation between observed and calculated frequencies, the better the calculated F^4 eigenvectors describe the extent of vibrational mixing. Since we are dealing with anharmonic (i.e. real) vibrations, a force field which models the observed vibrations of the molecule is better than one which uses vibrational frequencies corrected for anharmonicity. The F^4 is an excellent way of approaching this. (c) The assumption that the dipole moment change on vibration is along the MCO axis. Whilst in many situations this must be so on symmetry grounds, it may well not be true in general. We comment further on this point below. As a demonstration of the beauty of the intensity/force field method in general however we show Poliakoff's attractive computer simulated spectrum of $Cr(CO)_5CS$ compared to an (unretouched!) observed spectrum in Fig. 7 [79]. In Fig. 8 we show the spectroscopic evidence for the assignment of the C_{3v} structure and not the D_{2d} structure to the $Fe(CO)_4^-$ molecule. Both the frequency and intensity fit are conclusively in favor of the C_{3v} structure.

(iv) Description of the 'carbonyl' vibrations

We have used the description 'dipole moment change of the CO group on vibration' for the function μ'. In fact from the result of eqn. 16 the 'CO stretch' contains a sizeable admixture of MC stretching. (If the 'CO stretch'
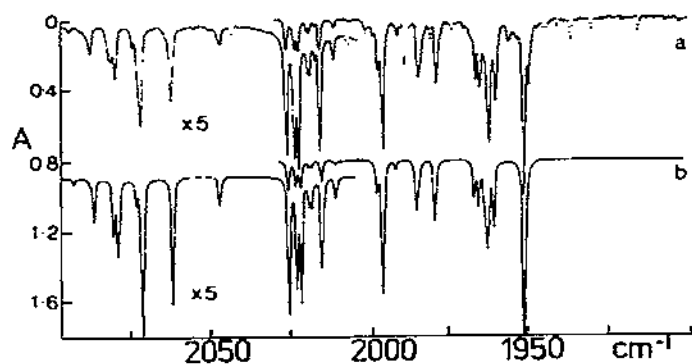
Fig. 7. (a) Observed and (b) computer simulated spectra of $Cr(^{12}CO)_{5-z}(^{13}CO)_z CS$ ($z = 0$—5) molecules trapped in a CH_4 matrix at 20 K. The same half width was used for all the bands in the simulated spectrum which makes the calculated high frequency bands slightly stronger than they should be. The dashed lines in (a) are due to a $Cr(CO)_6$ impurity. (From ref. 79 with permission.)
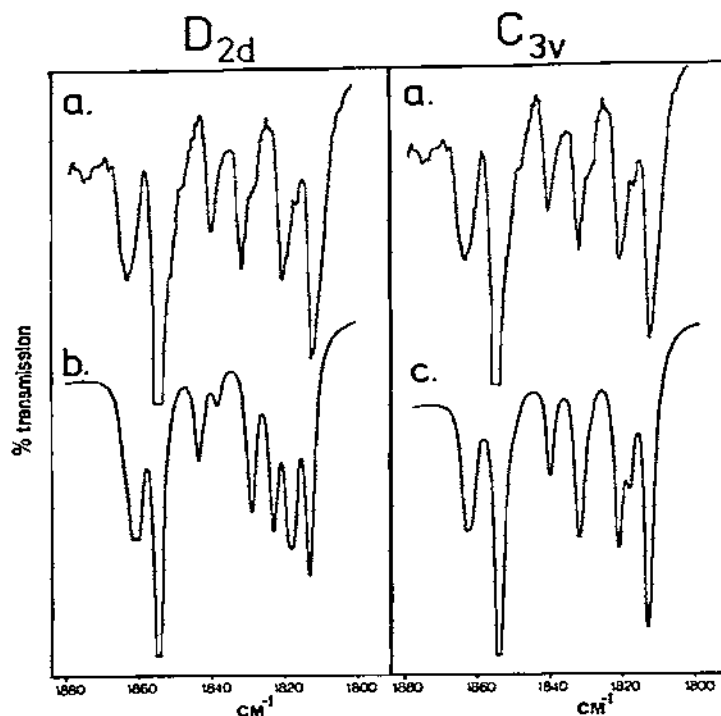

Fig. 8. (a) Observed spectrum in Ar at 12 K; (b) Computer simulated spectrum for the D_{2d} model ($\alpha = 132°$). (c) Computer simulated spectrum for C_{3v} model of $Fe(^{12}CO)_{4-z}(^{13}CO)_z^-$ ($z = 0$—4) molecules. (Adapted from ref. 68.)

were purely due to CO stretching then $L_{21} = 0$). Using the notation of eqn. 12 the derived dipole moment associated with the 'CO stretching' is given by

$$\frac{\partial \mu}{\partial Q_1} = \frac{\partial \mu}{\partial R_{CO}} L_{11} + \frac{\partial \mu}{\partial R_{MC}} L_{21} \tag{34}$$

Substitution of values for $\partial \mu / \partial R$ derived from a study of Ni(CO)$_4$ [65] gives eqn. 35 where it is apparent that the intensity of a 'CO stretch' contains significant contributions from the dipole moment change of the MC internal mode via the cross term. It is important to remember that even though the vibra-

$$\text{intensity} \propto 0.2504\ \mu'^2_{MC} + 0.7496\ \mu'^2_{CO} - 0.8665\ \mu'_{MC}\mu'_{CO}$$
$$= \qquad 4.76 \qquad + 58.31 \qquad + 33.32 (DA^{-1})^2 \tag{35}$$

tional frequency of the carbonyl stretch is dominated by the electronic properties of the CO oscillator the actual description of the normal mode involves considerable mixing with the MC oscillator.

In the approximation for λ_{CO} of eqn. 17 the mass of the central metal atom does not occur. This is simply because its reciprocal mass is much smaller than that of either carbon or oxygen. (Indeed one derivation [80] of eqn. 17 starts off from the assumption that μ_M is very small.) The obvious disadvantage of this fact is that it is usually impossible to tell from the carbonyl stretching vibrations, how many metal atoms are present in the complex, although several studies have concentrated on measuring metal atom isotope shifts in the low frequency region [81,82]. These studies however have been on stable carbonyls.

Values of the carbonyl stretching force constants and also bond—bond interaction force constants have long been related to the electronic structure of the molecule. Whilst this may be a valid procedure for the GQVFF potential constants, caution should be exercised with the F^4 constants. In general the value of k_{CO} is slightly smaller than f_{CO}, but the largest percentage differences between the two force fields occurs for the interaction force constants which are very sensitive to the nature of the approximations made. Great debate has raged in the past over the chemical significance of these force constants and we shall not discuss this further except to draw attention to some recent very remarkable results concerning the F^4 method. Timney has found [83] firstly that the interaction force constant $k_{CO,CO}$ between two CO groups with a CMC angle θ may be written as a very simple function of k_{CO} and the angle θ. Secondly, given the k_{CO} force constant for the MCO molecule (available from matrix studies for a large number of metals) the force constants in an M(CO)$_y$ molecule may be simply calculated if the angles between the ligands are known. Thus, incredibly, just knowing k_{CO} for the parent MCO molecule the entire IR and Raman spectrum of the molecule may be quite closely predicted, with a small number of parameters applicable to all carbonyl systems. Interestingly the same method does not apply for GQVFF constants .

(v) Results for ternary systems
Analysis of the vibrational problem for the carbonyl part of the Cr(CO)$_5$CS

molecule [79] led to an accurate determination of the potential constants and eigenvectors of the F^4. The analysis of IR intensities in the carbonyl region led to a value of the bond angle θ (6) of 82.8° when the molecule is

$$\theta \quad \underline{6}$$
CS
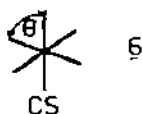
expected to have a bond angle very close to the regular octahedral value of 90°. (No crystal structure determination exists at the moment.) A similar result is found by analysis of the IR intensities in $\eta^5 CpMn(CO)_2CS$ where the calculated angle is 98.3° between the CO groups, substantially different from the observed angle of 92° [79,84]. Analysis of the vibrational/intensity problem for the new species $Mo(CO)_5N_2$ made in a matrix led to similar results [85]. For the latter species sufficient vibrational data were available to partly include the N_2 into the F^4 as a pseudo-CO ligand. Vibrational frequency shifts were observed in the high frequency 'CO' stretch on $^{14}N_2/^{15}N_2$ substitution confirming the presence of the R_{NN} internal mode in the high frequency a_1 normal mode of the $Mo(CO)_5$ unit. On inclusion of coupling between N_2 and CO vibrations the bond angle became nearer the octahedral value. No such evidence for CO/CS mixing was observed in the thiocarbonyl case. This result is analogous to similar failures in the carbonyl intensity method in the stable molecules $Fe(CO)_4PR_3$ where comparative X-ray crystallographic data are available. Taking the data from ref. 87 and using the methods outlined in this section bond angles very much less than 90° are found for these species [78]. In ref. 87 itself the ρ parameter of Brown and Darensbourg obscures this fact. Intriguingly, the corresponding $Fe(CO)_4 P(OR_3)_3$ systems behave normally. Here ρ is much smaller than for the phosphines. These results can be explained if the dipole moment change on vibration does not occur parallel to the MCO axis in the $Cr(CO)_5CS$ and $Fe(CO)_4PR_3$ examples. But why this occurs in the phosphine but not in the phosphite series is a puzzle. There are clearly features of the IR intensity problem which we do not completely understand at present, but the method seems good at least for binary systems or carbonyls containing in addition σ-donor ligands only.

(vi) Sideways or end-on bound ligands

One vital piece of structural information concerning the newly formed species is whether the diatomic ligand is bound in the end-on (monohapto) or sideways (dihapto) mode (7). The vibrational spectrum can in some cases give

$$M-N-N \qquad \begin{array}{c} N-N \\ \diagdown \diagup \\ M \end{array} \qquad \underline{7}$$
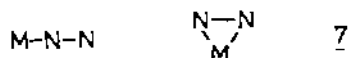
a definitive answer. Figures 9 and 10 show the spectra obtained by Ozin and co-workers on cocondensing Ni atoms [87] and Co atoms with a mixture of $^{14}N_2$, $^{14}N^{15}N$ and $^{15}N_2$. The number of IR bands observed shows conclusively
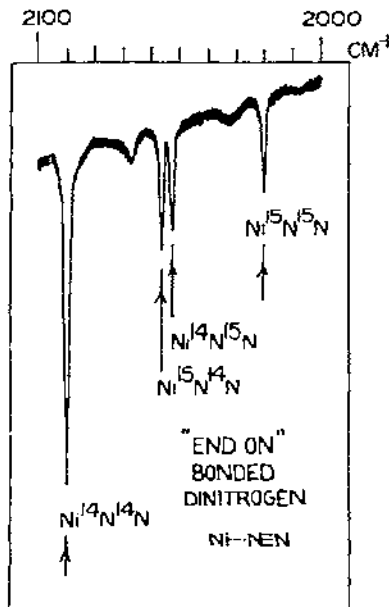
Fig. 9. IR spectrum of Ni^pN^qN (p, q = 14, 15) molecules in a solid N_2 matrix showing the split central component of the spectrum. (From ref. 87 with permission.)
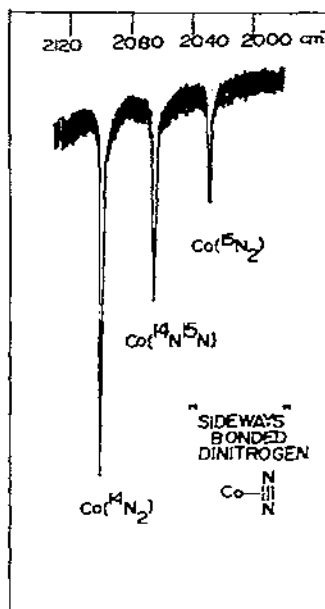
Fig. 10. IR spectra of Co^pN^qN (p, q = 14, 15) molecules in a solid N_2 matrix showing the unsplit or unresolved splitting of the central component of the spectrum. (From ref. 87 with permission.)

that new metal/N_2 complexes have been formed and specifically that only one N_2 unit is involved, i.e. the species are most likely to be CoN_2 and NiN_2. The central feature in the nickel case is split into two, conclusively showing that in this case the N_2 is bound end-on. The two bands correspond to the $Ni^{14}N^{15}N$ and $Ni^{15}N^{14}N$ molecules which have slightly different NN stretching frequencies. The CoN_2 species was initially claimed to be sideways bound because of the absence of such a splitting. Whereas in the monohapto structure two different molecules result (8), in this geometry the two possible arrangements (9) are identical. However, the absence of an observable splitting

$$M{-}^{14}N{-}^{15}N \qquad M{-}^{15}N{-}^{14}N \qquad 8$$

$$^{14}N{-}^{15}N \diagdown_M \qquad ^{15}N{-}^{14}N \diagup_M \qquad 9$$
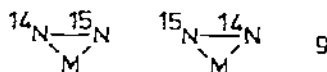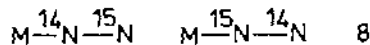
in this case does not allow distinction between the sideways bound arrangement and the end-on arrangement with an unobservably small splitting. From the F^4 result of eqn. 18 the two end-on possibilities will have the same NN

stretching frequency since only the reduced mass of the $^{14}N^{15}N$ unit appears in the expression for the frequency. The splitting arises as a consequence of the x terms in eqn. 17, the anharmonicity affecting both molecules very nearly equally. From this equation the splitting is proportional to xf_{MN} — $f_{MN,NN}$ which could well be close to zero. A rather attractive example of mono and dihapto species together in the same molecule is $\eta^2O_2Ni\eta^1N_2$ [88] where the isotopic $^{14}N^{15}N$ band is split into two (clearly $^1\eta$) but the $^{16}O^{18}O$ band is not split (indicating the *possibility* of $^2\eta$).

D. EXPERIMENTAL STUDIES ON MATRIX ISOLATED CARBONYLS AND RELATED SPECIES

In this section we discuss experimental studies on matrix isolated carbonyls, dinitrogen, dioxygen and hydrocarbon complexes. These have been made by photolysis of stable precursors in inert gas matrices and organic glasses and by metal atom cocondensation methods as we discussed above. There is not the space to review each contribution to this fascinating field in depth and so we have assembled data on these species in Table 2. In particular we are interested in the characterization via geometry determination of the new species and in column 3 note the degree of sophistication and quality of the structure determination. This varies from the very crude — the observation of new infra-red bands in a relevant spectral region — to the employment of the full power of the methods described above. The labels appearing in column 3 describe the quality of the characterization in the following way.

(a) The observation of new IR bands in the carbonyl stretching region or example is good evidence that some new $M_x(CO)_y$ species has been formed.

(b) By the study of the growth and decay curves associated with the new absorptions, bands may be assigned to one particular species. The relative number of coordinated ligands is estimated in the atom method by the temperature and ligand concentration dependence of the intensity of the new bands. Bands due to ML_y species where $y = 1, 2$ are produced at low temperatures and with dilute matrices. Species with a larger number of coordinated ligands are produced on warming the matrix when diffusion of L may occur. Use of a more concentrated matrix will achieve a similar result on cocondensation. With photolysis methods ML_{y-1} species are produced first on photolysis of the ML_y parent. Given the number, frequency and this other information about the new bands, only a certain number of ML_y species with a limited number of geometries is possible.

(c) The use of isotopes is the only really good way to pinpoint the number of coordinated ligands.

(d) Refinement of a vibrational force field may sometimes lead to a definitive geometry e.g. T_d for a four coordinate system or sometimes leave one geometrical degree of freedom undetermined (e.g. in C_{3v}).

(e) Use of the IR intensity method where applicable will give a numerical value for the bond angles in the system.

TABLE 2

Species	Method of preparation	Means of characterization	Comments	Ref.
Ti(CO)$_6$	Ti atoms + CO	IR (a)	significant distortion from octahedral $\nu(t_{1u})'$ split by 40 cm^{-1}	93
Ti(N$_2$)$_6$	Ti atoms + N$_2$	IR (a)	As Ti(CO)$_6$	93
Ti$_2$(CO)$_y$	Ti atoms + CO	IR (a)	no evidence for bridging CO groups	93
VCO	V atoms + CO	IR (d) ^{13}CO	very high ν(CO). C_s structure suggested [but see ref. 43]	94, 95
V(CO)$_2$	as above	as above	three different molecules identified possibly of C_{2h}, C_{2v} and $D_{\infty h}$ symmetry e.g. C—V—C cf. VCO [could also be due to site effect, see Au(CO)$_2$, Ni(O$_2$)$_2$]	94
V(CO)$_3$	as above	as above	no high frequency a_1 mode observed C_{3v} or D_{3h}	94
V(CO)$_4$	as above	IR (b)	overlapping bands preclude isotopic analysis T_d or D_{4h}	94
V(CO)$_5$	as above	IR (b)	D_{3h} from number of IR bands	94, 36
V(CO)$_6$	as above	IR (b)	not as distorted as Ti(CO)$_6$	96, 97
V(N$_2$)$_6$	V atoms + N$_2$	IR (b)	closely octahedral	98
V$_2$(CO)$_{12}$	V atoms + CO	IR (c) ^{13}CO	extensive isotopic analysis prevented by band overlap	96, 97
V$_2$(N$_2$)$_y$	V atoms + N$_2$	IR (b)	bridging CO groups observed y may be 12	98
Nb(N$_2$)$_y$	Nb atoms + N$_2$		cited in ref. 101	37
Ta(CO)$_y$ (y = 1—6)	Ta atoms + CO	IR (c) C^{18}O	tentative assignments	37
CrCO	Cr atoms + CO	IR (a)		95
M(CO)$_3$ (M = Cr, Mo, W)	in situ photolysis of Mo(CO)$_6$	IR (e) ^{13}CO	C_{3v} CMC angle 105° for Mo analog	77
M(CO)$_4$	as above	as above	C_{2v}, CMC angles 107°, 174° in Mo analog	77
M(CO)$_5$	as above	IR (e) ^{13}CO	C_{4v}, CMC angle (axial/basal) Cr, 91° (Xe), 93° (CH$_4$); 96° (Ar); Mo 91° (CH$_4$); W, 94° (CH$_4$) see text	53, 99—101, 3, 54

27

Species	Method of generation	Technique	Comments	Ref.
W(CO)₅	in situ photolysis of W(CO)₅ pyridine	IR (a)	photochromism found	102
M(CO)₅	M atoms + CO	IR (e) ^{13}CO	debate over geometry. C_{4v} is correct exhaustive F^4 analysis	52,54
M(CO)₆	stable molecule	IR (e) ^{13}CO, $C^{18}O$ $^{13}C^{18}O$, ˣCr		53, 64, 66, 81
M(CO)₅⁻	in situ VUV M(CO)₆; K, Na atoms + photolysis of M(CO)₆; electron bombardment	Ir (e) ^{13}CO	C_{4v} geometry angle ~95°	5, 68, 103
M(CO)₅N₂	in situ photolysis of M(CO)₆/N₂, N₂/Ar	R, IR (e) ^{13}CO	C_{4v}, N₂ monohapto, loses N₂ on near UV irradiation	85
Cr(CO)₅CS	stable molecule	IR (e) ^{13}CO	OCM CO angle ~83° from F^4 see text	16, 79
Cr(CO)₄CS	in situ photolysis of Cr(CO)₅CS	IR (e) ^{13}CO	C_{4v} and C_s forms identified inconvertible on visible photolysis	16, 79
Cr(N₂)₁₋₆	Cr atoms + N₂	IR (b)	$D_{\infty h}$, D_{3h}, D_{4h} or T_d, C_{4v} structures suggested for Cr(N₂)₂ to Cr(N₂)₅ respectively	104
Cr(N₂)₆	as above	as above	electronic spectrum	104, 164
Cr(O₂)₂	Cr atoms + O₂	IR (d)	uncertainty as to mono or dihapto arrangement	105
Mn(CO)	Mn atoms + CO	IR (e)	C_{4v}	95
Mn(CO)₅	as above	IR (b)	C_{3v} H Mn(CO)₄, photochromism	27
H Mn(CO)₄,₅	in situ photolysis of H Mn(CO)₅	IR ^1H, ^2H (b)	evidence for insertion	106
R Mn(CO)₅,₄ (R = CH₃, CF₃)	in situ photolysis of R Mn(CO)₅			107
Mn(CO)₃,₂NO	in situ photolysis of Mn(CO)₄NO	IR (b)	possible loss of 2 CO groups from parent	108
Mn(CO)₄NO	stable molecule	IR (c)	equatorial NO confirmed	125
Mn₂(CO)y	Mn atoms + CO	IR (d)		27
Re(CO)₅	Re atoms and CO	IR (c)	square pyramidal	121
FeCO	Fe atoms + CO	IR (a)		95
Fe(CO)₃	in situ photolysis of Fe(CO)₅	IR (e) ^{13}CO	C_{3v}, ∠C−Fe−C 108 ± 3° initial claim of C_{3v} structure incorrect.	10
Fe(CO)₄	as above	IR (e) ^{13}CO	C_{2v} with O−Fe−C angles of ~120° and ~145°	8, 9
	as above	MCD	triplet ground state	109

TABLE 2 (continued)

Species	Method of preparation	Means of characterization	Comments	Ref.
$Fe(CO)_5$	stable molecule	IR		8, 9, 110
$Fe(CO)_4^-$	in situ VUV $Fe(CO)_5$, Na atoms + photolysis $Fe(CO)_5$, high energy electrons + $Fe(CO)_5$	IR (e)	C_{3v}, C—Fe—C angle $\sim 100°$	5, 68
$Fe(CO)_2Cb$	in situ photolysis $Fe(CO)_3Cb$	IR (a)	possible product contains $CH_2=CH-C\equiv CH$	111
$Fe(CO)_4C_2H_4$	in situ photolysis $Fe(CO)_5$ in Ar/C_2H_4	IR (b)		112
$Fe(CO)_4N_2$	as above in N_2	IR (b)	C_{3v}, axial N_2	9, 113
$Fe(CO)_4Q$ $Q = Xe, CH_4$	as above in Q	IR (e) ^{13}CO	C_{2v} equatorial Q	9
$Fe(CO)_4CH_4$	laser IR photolysis of $Fe(CO)_4$	IR (a)	IR laser induced reaction	184
$FeCO(NO)_2$	in situ photolysis of	IR (b)		114
$FeCON_2(NO)_2$ $Fe(N_2)_2(NO)_2$	$Fe(CO)_2(NO)_2/N_2/Ar$			
$Fe_2(CO)_{8,9}$	in situ photolysis of $Fe_2(CO)_9$	IR (b)	bridged and non-bridged forms found for $Fe_2(CO)_8$	115
$Fe_3(CO)_{12}$	stable molecule	IR	spectrum different to that in solution. Doubly bridged C_{2v} structure suspected	116, 117
Fe_2N_2	Fe atoms/N_2	IR (a) Mössbauer	N_2 reacts with Fe_2 not Fe	118
FeO_2	Fe atoms and O_2	IR (b)		211
$Ru_3(CO)_{12}$	stable molecule	IR	spectra very similar to those in solution	116,117
$Os(CO)_4$	in situ photolysis $Os(CO)_5$	IR (b)	more than one $\nu(CO)$ assigned, not D_{4h}, see text	9
$Os(CO)_2(NO)_2$	in situ photolysis of $Os(CO)_5/NO$	IR (b)	spectra similar to those in solution	119
$Os_3(CO)_{12}$	stable molecule	IR		116,117
CoCO	Co atoms + CO	IR (d) ^{13}CO, $C^{18}O$	$C_{\infty v}$	95, 120
$Co(CO)_2$	as above	as above	$D_{\infty h}$	120
$Co(CO)_3$	as above	as above + ESR	C_{3v} or D_{3h}, axially symmetric g tensor	120
$Co(CO)_4$	as above	as above + R	ESR gives mixture of D_{2d}, C_{3v} in Ar, only C_{3v} in CO	120, 122
$Co(CO)_3NO$	in situ photolysis $Co(CO)_3NO/CO$	IR (e)	C_{3v}, C—Co—C angle $\sim 100°$	119

$Co(N_2)$	Co atoms + N_2	IR (c) $^{14}N^{15}N$, $^{15}N_2$	suggested to be dihapto but see text	87
$Co(CO)_2NO$,	in situ photolysis	IR (c)		204
$Co(CO)_y(N_2)_{3-y}NO$	$Co(CO)_3NO/Ar/N_2$			
$Co_2(CO)_8$	Co atoms + CO	IR (a)	produced with high concentrations of metal atoms	120
$Co_2(CO)_7$	stable molecule	IR (a)	third isomer found, no bridging groups	199
$Rh(O_2)_{1,2}$	in situ photolysis	IR (a)	no bridging groups	200
$Rh_2(O_2)_n$	Rh atoms and O_2	IR (c) $^{18}O_2$, $^{16}O^{18}O$	sideways bound O_2	206
$Rh_3(O_2)_m$	as above	as above	bonding models for chemisorbed O_2	207
RhN_2	Rh atoms + N_2	IR (d) $^{14}N^{15}N$, $^{15}N_2$	$C_{\infty v}$	7
$Rh(N_2)_2$	as above	as above	$D_{\infty h}$	7
$Rh(N_2)_3$	as above	IR (b)	difficult to characterize	7
$Rh(N_2)_4$	as above	IR (d) $^{14}N^{15}N$, $^{15}N_2$	D_{2d}	7
$Rh_2(CO)_8$	Rh atoms + CO	IR (b)	no evidence for bridged form	123
$Ir_2(CO)_8$	Ir atoms + CO	IR (b)	as above	123
NiCO	Ni atoms + CO	IR (d) ^{13}CO	$C_{\infty v}$	37
$Ni(CO)_2$	as above	as above	$D_{\infty h}$	37
$Ni(CO)_3$	as above	as above	D_{3h}	37
	in situ photolysis of $Ni(CO)_4$	IR (b)	C_{3v} structure incorrect, matrix too concentrated	124
$Ni(CO)_4$	Ni atoms + CO	IR, R		126
	stable molecule	IR (c) ^{13}CO, ^{58}Ni, ^{60}Ni, ^{62}Ni, ^{64}Ni	$\nu(Ni-C)$ and NiCO studied	82
$Ni(N_2)_y$	Ni atoms + N_2	IR (c)	incorrect formulation of y	38, 39
$Ni(N_2)$	as above	R, IR (d) $^{14}N^{15}N$, $^{15}N_2$	$C_{\infty v}$	127
$Ni(N_2)_2$	as above	as above	$D_{\infty h}$	127
$Ni(N_2)_3$	as above	as above IR (e)	D_{3h}	127
$Ni(N_2)_4$	as above	as above	T_d or slightly distorted	127
$Ni(CS)_y$	Ni + CS (μwave discharge)	IR	$\nu(CS)$ above free CS [no more data]	95
$Ni(COS)_y$	Ni + COS	IR	[no data available]	95
$Ni(CS_2)_y$	Ni atoms + CS_2	IR (b)	three products probably $Ni(CS_2)_{1-3}$	130

TABLE 2 (continued)

Species	Method of preparation	Means of characterization	Comments	Ref.
$Ni(CO_2)_y$	Ni atoms + CO_2	IR (a)	erroneous, bands due to $Ni(N_2)_y$	24, 25
$NiX_2 \cdot L_2$ X = F, Cl L_2 = CO, N_2, NO, O_2 (Also data for Ca, Cr, Mn, Cu, Zn)	NiX_2 in L_2 matrix	IR (a)	positive $\nu(CO)$ shifts 10—30 cm^{-1}	128, 129
$M(O_2)_{1,2}$ M = Ni, Pd, Pt	Ni atoms + O_2	IR (d) $^{16}O^{18}O$, $^{18}O_2$	dihapto O_2, D_{2d} structure for $M(O_2)_2$	91, 92
$MO_2(N_2)_{1,2}$ M = Ni, Pd, Pt	M atoms + O_2/N_2	IR (d) $^{14}N^{15}N$, $^{15}N_2$ $^{16}O^{18}O$, $^{18}O_2$	dihapto O_2, monohapto N_2	88
$Ni(CO)_3N_2$	in situ photolysis $Ni(CO)_4/N_2$	IR (a)	monohapto N_2	6
$Ni(CO)_z(N_2)_{4-z}$	Ni atoms + CO/N_2	IR (d) ^{13}CO $^{15}N_2$	all tetrahedral. Analysis of σ-donor and π-acceptor properties of CO, N_2 ligands	131
$Ni(C_2H_4)_{1}-3$	Ni atoms + C_2H_4	IR (b)	$Ni(C_2H_4)_2$ D_{2h} structure	132
$Ni(C_2F_4)_n$	Ni atoms + C_2F_4	IR (a)	best described as a series of perfluoro-metallocyclopropane—perfluoroethylene complexes	208
η^5 Cp NiNO	in situ photolysis	IR (a)	new low frequency $\nu(NO)$ on photolysis. Ionic structure CpNi:⁻ NO⁺ or bent MNO group suggested.	138, 139
$Ni(CO)_3$	VUV photolysis of $Ni(CO)_4$ high energy electron bombardment	IR (d) ^{13}CO	D_{3h}	5, 68
$Ni_{(c)}N_2$	Ni atoms + N_2	IR (d) $^{15}N_2$		38, 39
$Ni_{(c)}CO$	Ni atoms + CO	IR (a)		140
$Pd(CO)_{1-4}$	Pd atoms + CO	R, IR (b)	spectra consistent with highest symmetry structures in each case	126, 133
$Pd(CO)_4$	as above	IR (e) $C^{18}O$	T_d	134
$Pd(N_2)_{1,2}$	Pd atoms + N_2	IR (d)	$C_{\infty v}$ and $D_{\infty h}$ geometries	127

Species	Preparation	Technique	Notes	Ref.
Pd(N₂)₃	as above	IR (e) ¹⁵N₂	slightly distorted D_{3h}, no tetrakis species formed	127, 135
Pd(C₂H₄)₁₋₃	Pd atoms + C₂H₄	IR (d) ¹³C₂H₄	probably D_{2h} structure for Pd(C₂H₄)₂ and D_{3h} for Pd(C₂H₄)₃	136, 137
PtCO	Pt atoms + CO	IR (d) ¹³CO	$C_{\infty v}$	126, 141
Pt(CO)₂	as above	as above	$D_{\infty h}$	126, 141
Pt(CO)₃	as above	as above IR (e)	D_{3h}	126, 141
Pt(CO)₄	as above	as above	T_d	126, 141
PtN₂	Pt atoms + N₂	IR (d) ¹⁴N¹⁵N, ¹⁵N₂	$C_{\infty v}$	142, 143
Pt(N₂)₂	as above	as above	one study suggests dihapto N₂	142, 143.
Pt(N₂)₃	as above	as above	D_{3h}	142, 143
CuCO	Cu atoms + CO	IR (d) ¹³CO, C¹⁸O	$C_{\infty v}$	144
Cu(CO)₂	as above	as above	$D_{\infty h}$	144
Cu(CO)₃	as above	as above	D_{3h}	144
Cuₓ(CO)ᵧ	as above	as above	x probably 2	144, 145
Cu(C₂H₄)₁₋₃	Cu atoms + C₂H₄	IR	π-bonded C₂H₂ (cf. Al) Cu(C₂H₂)₂	154
Cu(C₂H₂)₁,₂	Cu atoms + C₂H₂	ESR	probably D_{2h}	146
Cu₆N₂	Cu atoms + N₂	IR (d)	ν high ν(NN)	39
Cu(O₂)₂	Cu atoms + O₂	IR (d)		105
Cu(C₂H₄)ₙ n = 1–0	Cu atoms and C₂H₄	IR (a)	Complexes unstable compared to Ni analogs	209
Cu(CO)ₘ m = 4, 6				
AgCO	Ag atoms + CO	IR (d) ¹³CO	$C_{\infty v}$	147
Ag(CO)₂	as above	as above	$D_{\infty h}$	147
Ag(CO)₃	as above	ESR, as above	D_{3h}	147
Ag₂(CO)₆	annealing above	IR	study of diffusion process	148
MO(M = Cu, Ag, Au)	M atoms + O₂ (followed by photolysis)	IR	included in this review because of the novel method of production	210
Ag(O₂)₁,₂	Ag atoms + O₂	IR (d) ¹⁶O¹⁸O, ¹⁸O₂	best formulated as Ag⁺O₂⁻, Ag⁺O₄⁻	149
Ag(CO)O₂	Ag atoms + O₂/CO	IR (d) ¹⁶O¹⁸O, ¹⁸O₂ ¹³CO, ¹³C¹⁸O	best formulated as AgCO⁺O₂⁻	150
Ag(CO₂)		IR (e) ¹³CO₂		212
Au(CO)	Au atoms + CO	IR (d) ¹³CO, C¹⁸O, ¹³C¹⁸O	bonding model for adsorbed CO₂ $C_{\infty v}$	89

TABLE 2 (continued)

Species	Method of preparation	Means of characterization	Comments	Ref.
Au(CO)$_2$	as above	as above	$D_{\infty h}$. In pure CO the isocarbonyl/carbonyl structure CO. Au. CO proposed [see text] No tricarbonyl	89
AuO$_2$	Au atoms + O$_2$	IR (c) $^{16}O^{18}O$, $^{18}O_2$	best formulated as AuO$_2^-$ not Au$^+$O$_2^-$	151
Au(CO)$_2$O$_2$	Au atoms + CO/O$_2$	IR (c) ^{13}CO, $C^{18}O$, $^{13}C^{18}O$, $^{16}O^{18}O$, $^{18}O_2$	peroxyformate structure proposed, see text	152
AuC$_2$H$_4$	Au atoms + C$_2$H$_4$	IR (c) ^{13}C		153
M(CO)$_y$ M = Pr, Nd Gd, Ho, Eu, Er, Yb	M atoms + CO	IR	some isotopic data, no evidence for values of y	155, 156 205
U(CO)$_y$	U atoms + CO	IR (b)		157
Al(CO)$_2$	Al atoms + CO	IR (d)	C_{2v} molecule. 1st non-transition metal carbonyl	34
AlC$_2$H$_2$	Al atoms + C$_2$H$_2$	ESR	H$\diagdown$C=CH, Al$\diagup$	158
M$_x$(CO)$_y$ M = Ge, Sn	M atoms + CO	IR	possible formation of MCO, analogs of CCO	159
K$_x$(CO)$_3$	K atoms + CO	IR (c)	C_{3v} arrangement of CO groups	160
SnCl$_2$·L$_2$ PbF$_2$·L$_2$(L$_2$ = CO, NO, N$_2$), PbX$_2$·CO (X = Cl, Br, I)	MX$_2$ + L$_2$ in Ar	IR (c)	ν(CO) shifted to higher frequency	161

A survey of Table 2 shows that all the good structural results have been for the carbonyl and dinitrogen cases. For O_2 and hydrocarbon complexes the analysis has usually stopped short of the isotopic substitution point. For the former complexes at least there is no excuse today for not performing a good structural characterization of the new molecule.

One species which chemists have sought for many years is the isocarbonyl (O-bonded) moiety. In several molecules both O and C atoms are attached to a metal (M'—O—C—M) but no species have been found containing the M—O—C unit. The matrix environment should surely be one the places to look for such an unfavorable arrangement. There have been several attempts, the latest being the proposition that CO · Au · CO has been characterized in solid CO matrices [89]. The spectra of this species are exceedingly similar to those of $Au(CO)_2$ itself ($D_{\infty h}$ structure) but differ by the presence of a weak high frequency vibration in the IR and the splitting of the bands which would be assigned to $Au(^{12}C^{16}O)(^{13}C^{16}O)$. The observed splitting is totally consistent with the coordination of two *slightly* different CO groups. Analysis using the F^4 method of the carbonyl region of the spectrum by this author for this review shows that the observed spectrum may be well described by a $Au(CO)_2$ species with CO stretching force constants differing by less than 0.1 mdynes $Å^{-1}$! This is hardly the difference in force constant expected for the isocarbonyl v. carbonyl. In addition the standard deviation of the present analysis is very much less than 1 cm^{-1} whereas the published analysis for these same bands on the carbonyl/isocarbonyl model is around 18 cm^{-1}! An earlier (unpublished) analysis of the Au/CO system also arrived at the conclusion that the splitting observed in the spectra of $Au(CO)_2$ isolated in pure CO was due to a slight inequivalence of the two CO groups most likely demanded by the CO crystal structure [90]. Interestingly a study of $Ni(O_2)_2$ showed very similar behavior [91,92] of the isotopic spectrum. Here of course there can be no alternative to the matrix induced inequivalence of the two O_2 units.

E. THE SHAPES OF BINARY CARBONYL AND DINITROGEN COMPLEXES

An early incentive for matrix isolation studies on binary transition metal carbonyls and dinitrogen complexes in matrices was the determination of the structures of these species as a function of the electronic configuration of the central transition metal atom. Thus $Mo(CO)_4$ provided the first four-coordinate molecule with the low spin (ls) d^6 electronic configuration, and $Fe(CO)_3$ the first three-coordinate high spin (hs) d^8 molecule.

The structures of main group molecules have for many years been approached using the VSEPR ideas of Nyholm and Gillespie [162,163]. However in the years following the formulation of this concept, molecular orbital approaches have become more widely accepted and understood. Today we look there for convincing explanations of facets of molecular structure. Gillespie suggested [162] that, since the metal d orbitals were involved in π-bonding the geometry of an $M(CO)_y$ species would be determined by the

VSEPR properties of the y σ-pairs lying to low energy; i.e. all tetracarbonyls would be tetrahedral, all tricarbonyls trigonal planar etc. However, he also anticipated that problems would arise if the electronic configuration of the metal were not spherically symmetrical and the geometry would distort from the VSEPR one. If we add to Table 2 the square planar geometry of the related species $Ni(CN)_4^{2-}$ (is d^8) this is certainly true. For four-coordinate species there are no fewer than six different geometries (D_{4h}, T_d, C_{2v} (twice), C_{3v}, D_{2d}) for molecules with different d electron configurations.

Figure 11 shows a familiar molecular orbital diagram for a GpVl hexacarbonyl e.g. $Cr(CO)_6$. A similar diagram applies to the related species $Cr(N_2)_6$. This diagram was constructed so as to be consistent with the observed electronic spectrum of these molecules. The metal d orbitals are split apart in energy by the octahedral field into two sets, separated by the splitting parameter Δ. This splitting is large compared to that in many other systems e.g. halide, because the CO ligand is a π-acceptor. Empty orbitals on the ligands lying higher in energy than the metal d-orbitals are of the correct symmetry to stabilise the t_{2g} set. With six electrons in the t_{2g} orbitals two sorts of electronic transition are observed. Specifically for $Cr(CO)_6$, to low energy (389 nm) a weak absorption ($\epsilon = 3400$) is ascribed to the configuration change $(t_{2g})^6 \rightarrow (t_{2g})^5(e_g)^1$, the $d-d$ transition. To higher energy are the intense ($\epsilon = 85100$) charge transfer transitions $(t_{2g})^6 \rightarrow (t_{2g})^5(\pi^*)^1$. The former transition is Laporte forbidden and may only gain intensity by vibronic coupling. $d-d$ transitions in carbonyls of lower symmetry (e.g. C_{4v} $Cr(CO)_5$) are also Laporte forbidden but gain intensity by static d/p mixing. The charge transfer bands are always intense. There has recently been a matrix isolation study of
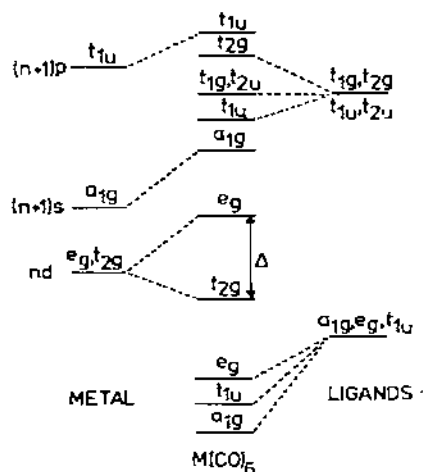

Fig. 11. A schematic molecular orbital diagram for an octahedral $M(CO)_6$ species, showing the σ- and π^*-orbitals on the ligands. For the sake of clarity the ligand π-orbitals have been left off the diagram.

the electronic spectra of $M(CO)_6$ and $M(N_2)_6$ species (M = Ti, V, Cr) [164].

The large gap between the e_g and t_{2g} sets bestows thermodynamic and kinetic stability on the molecule, and here lies the basis of the 18-electron (or effective atomic number) rule which is used so frequently in this field. It turns out that for most stable systems with strong field ligands, a total of 18 electrons are needed to fill the σ-donor orbitals of the ligands and leave enough left over to fill all the low energy central metal atom d orbitals such that there is a significant HOMO—LUMO gap. An exception to the 18-electron rule which has a ready explanation when viewed in this way is the series of stable 16-electron square-planar d^8 molecules where there is a large gap between $x^2 - y^2$ and the other d-orbitals. Parenthetically we also note that the 20-electron system $W(C_2H_2)_3CO$ contains two electrons in a σ-non-bonding orbital and so is not really a violation of the rule.

Excitation of an electron from t_{2g} to e_g in the $Cr(CO)_6$ example leads to population of a high energy orbital and rapid loss of CO (cf. eqn. 1). Similarly introduction of an electron externally leads to $Cr(CO)_6^-$ via dissociative electron capture by $Cr(CO)_6$. The d^7 and d^8 hexacarbonyls which would require population of the e_g set are not known. (There is a band observed in one experiment which is very tentatively assigned to $Mn(CO)_6$ [119].) The 18-electron rule in the binary carbonyl field gives an upper limit for y in the stable $M(CO)_y$ series as a function of d electron configuration. Interestingly however, although $Ni(CO)_4$, $Fe(CO)_5$ and $Cr(CO)_6$ are well known, recent Ti atom cocondensation experiments unearthed no evidence for $Ti(CO)_7$ [93]. The hexacarbonyl corresponded to the highest coordination number found. It seems to be a general rule with very few exceptions that carbonyl containing molecules do not exist with more than 18 electrons. One well characterized exception is the 20-electron Cu^1L CO where L is a macrocyclic ligand [165], although even here there is a chance that the ligand L is behaving non-innocently. For a general discussion of the electronic spectra and structure of carbonyl molecules see refs. 166 and 167.

For the geometries expected for these binary carbonyls we need to look at the results of molecular orbital calculations. There are several ab initio calculations on $Ni(CO)_4$ and some five- and six-coordinate species [170—172], but there are only two sets of calculations for a comprehensive selection of coordination numbers and d orbital configuration [173,174]. These are of the extended Hückel type and the results are given in Table 3. The two approaches differ only in parameterization and it is interesting to note that there are some differences in the lowest energy geometries predicted by the two methods. This must be ascribed to a quirk of the semi-empirical method itself but even so the general agreement between observed and calculated structures is quite good.

For the d^9 four-coordinate system both sets of calculations predict that the D_{2d} structure should be most stable but that the C_{3v} geometry is close in energy. Very interestingly IR data on $Co(CO)_4$ and $Fe(CO)_4^-$ in Ar matrices indicate a C_{3v} geometry [68,119] and ESR data on $Co(CO)_4$ show that in

TABLE 3

Calculated geometries of binary transition metal carbonyls by the extended Hückel method

d orbital population	I (ref. 127)	II (ref. 128)	Examples[a]
Coordination number 3			
d^5 22100	C_{3v} ($\theta = 63°$)	C_{3v} ($\theta = 58°$)	V(CO)$_3$ C_{3v} or D_{3h}
d^6 22200	C_{3v} ($\theta = 60°$)	C_{3v} ($\theta = 57°$)	Mo(CO)$_3$$C_{3v}$($\theta = 55°$)
22110	C_{2v} ($\alpha = 170°$)		
21111	D_{3h}		
d^7 22210	C_{2v} ($\alpha = 170°$) ($\theta = 90°$)	C_{3v} ($\theta = 63°$)	
22111	D_{3h}		
d^8 22220	C_{2v} ($\alpha = 175°$) ($\theta = 90°$)	C_{2v} ($\alpha = 172°$) ($\theta = 90°$)	
22211	C_{3v} ($\theta = 73°$)		Fe(CO)$_3$ C_{3v} ($\theta = 72 \pm 3°$)
d^9 22221	C_{2v} ($\alpha = 150°$)	C_{3v} ($\theta = 75°$)	Co(CO)$_3$ C_{3v} or D_{3h}
d^{10} 22222	D_{3h}	C_{3v} ($\theta = 82$)	M(L$_2$)$_3$ M = Ni, Pd, Pt L$_2$ = CO, N$_2$ D_{3h}
Coordination number 4			
d^5 22100	C_{2v}(100°, 160°)	C_{2v}(100°, 160°)	V(CO)$_4$ T_d or D_{4h}?
d^6 22200	C_{2v} (90°, 170°)	C_{2v} (95°, 165°)	Mo(CO)$_4$$C_{2v}$ (107,174°)
22110	D_{4h}		
21111	T_d		
d^7 22210	D_{4h}	C_{2v} (135°, 150°)	
22111	T_d		
d^8 22220	D_{4h}	D_{2d}(150°)	Ni(CN)$_4^{-2}$ D_{4h}
22211	C_{2v}(110°, 135°)		Fe(CO)$_4$ C_{2v} (~120°, ~145°)
d^9 22221	D_{2d} (132°)	D_{2d} (135°)	Fe(CO)$_4$, Co(CO)$_4$ C_{3v} ($\theta \sim 100°$). also Co(CO)$_4$ D_{2d}, Rh(N$_2$)$_4$ D_{2d}
d^{10} 22222	T_d	T_d	M(L$_2$)$_4$ M = Ni, Pd, Pt L$_2$ = CO M = Ni, L$_2$ = N$_2$ T_d
Coordination number 5			
d^5 22100	D_{3h}	C_{4v} ($\theta = 94°$)	V(CO)$_5$ D_{3h}?
d^6 22200	C_{4v} ($\theta = 93.5$)	C_{4v} ($\theta = 93°$)	W(CO)$_4$CS, Cr(CO)$_5$ C_{4v} (θ = variable)
22110	D_{3h}		
21111	D_{3h}		
d^7 22210	C_{4v} ($\theta = 98°$)	C_{4v} ($\theta = 98°$)	Mn(CO)$_5$, Re(CO)$_5$ C_{4v} Cr(CO)$_5^-$ ($\theta \sim 95°$)
22111	D_{3h}		
d^8 22220	D_{3h}	D_{3h}	Mn(CO)$_5^-$, Fe(CO)$_5$ D_{3h}
22211	C_{2v}		

Angles

C_{3v} C_{2v} $C_{2v} \cdot D_{2d}$ C_{3v} C_{4v}

[a] Only well characterized molecules appear in this column. A question mark follows some structures which are based on information not as good as the rest.

some environments it has a D_{2d} geometry [120]. The two forms must be close in energy.

For the high spin d^8 system (triplet) a distorted tetrahedron (C_{2v}) is expected for a four coordinate fragment but a square planar geometry for the low spin (singlet) form. The molecular orbital calculations include only orbital energy and are therefore unable to decide on the relative energies of singlet and triplet structures. (Such a determination would be difficult even at the ab initio level.) Fe(CO)$_4$ was found to have a C_{2v} structure and it was concluded on this basis to be a triplet. Recent MCD studies on matrix isolated Fe(CO)$_4$ have confirmed this conclusion [109]. Fe(CO)$_4$ is also predicted to have a C_{3v} geometry lying close in energy to the C_{2v} ground state structure. (In molecular orbital terms its origin is similar to the low lying C_{3v} geometry calculated for a d^9 species noted above.) Thermal rearrangement of Fe(CO)$_4$ induced by IR laser irradiation [175] of the carbonyl stretching bands, as we will describe later, probably occurs via a transition state closely related to this C_{3v} geometry. The triplet nature of Fe(CO)$_4$ is perhaps unexpected and has aroused some interest. The analogous d^8 cyanides (e.g. Ni(CN)$_4^{-2}$) are square planar singlets. In general the energy balance between singlet and triplet forms will be between an orbital term (promotion of an electron from z^2 to $x^2 - y^2$ of the square planar molecule) and the gain in exchange energy as the two electrons are unpaired. We noted above that the orbital part of this equation is likely to be large (CO is a high Δ ligand) which would not favor the triplet structure. The spin pairing contribution seems to win out. Of interest in this connection is the geometry of the congener Os(CO)$_4$. Here, since Δ will be larger and the spin pairing energy smaller, the balance should firmly put the singlet to lower energy. These speculations are all the more interesting since a very preliminary report of the Os(CO)$_4$ structure indicates that it may be similar to Fe(CO)$_4$ [9].

The object of the molecular orbital calculations is to view the energy changes on distortion of a molecule along various angular coordinates and locate the lowest energy structure. This is best done as a function of d-electron configuration by plotting the energies of the mainly metal d-orbitals as a function of geometry. The resultant diagrams, similar to those produced by Walsh for main group molecules, may then be used to view the vital effect of d-electron configuration on molecular geometry. An alternative way to regard the coordination geometry is to use the angular overlap model (AOM) which is finding increasing use in structural transition metal chemistry and has recently percolated into student texts. The method may be regarded as the molecular orbital equivalent of the crystal field model. We give a brief survey of the method here [176,177].

Second-order perturbation theory tells us that the energy of interaction of two orbitals ϕ_i and ϕ_j is proportional to the expression (36) where the numerator is simply $H_{ij} - S_{ij}\epsilon_i^{(0)}$. H_{ij} is the off-diagonal matrix element and S_{ij} the

$$\epsilon_i^{(2)} = \frac{|\langle\phi_i|H|\phi_j\rangle|^2}{\epsilon_i^{(0)} - \epsilon_j^{(0)}} \qquad (36)$$

overlap integral, between ϕ_i and ϕ_j, and $\epsilon_i^{(0)}$ and $\epsilon_j^{(0)}$ are the energies of the two orbitals before interaction. (In some instances in using this form of the perturbation approach we need to go to terms in fourth order to view geometrical preferences. We shall ignore the details of such sophistication in the treatment here.) Manipulation of eqn. 36 gives the result (37). The beauty

$$\epsilon_i^{(2)} \alpha S_{ij}^2 \qquad (37)$$

of the AOM is that S_{ij} may be written simply as a product of a constant term, dependent only on the bond length, and an angular term $f(\theta, \phi)$, dependent upon the location of orbital i relative to orbital j in space (38). θ, ϕ are the

$$S_{ij} = S_\sigma \cdot f_{ij}(\theta, \phi) \qquad (38)$$

standard polar angles defining their relationship. For the case of n ligand σ-orbitals surrounding a central metal atom some useful values of $f_{ij}(\theta, \phi)$ for ligand σ-metal d-overlap are shown in 10. Thus for a given geometry the energy of
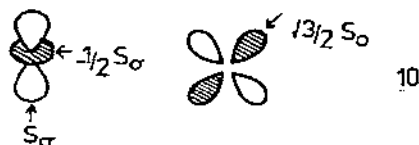
interaction of a given d-orbital (j) with the ligands may be calculated by combining eqns. 37 and 38 and summing (39). β_σ is the proportionality constant occurring in eqn. (37). Figure 12 shows molecular orbital diagrams for ligand

$$\epsilon_j^{(2)} = \beta_\sigma S_\sigma^2 \ \Sigma f_{ij}^2(\theta, \phi) \qquad (39)$$

σ-metal d-orbital interactions obtained by this method for three four-coordinate geometries. We assume for simplicity that the bonding partner (mainly ligand) receives as much stabilization as the antibonding partner (mainly metal d) does destabilization. All the bonding orbitals are filled with two electrons but the number of antibonding electrons depends upon the d-orbital configuration. Two electrons in an antibonding orbital will exactly cancel the stabilization conferred on the system with two electrons in the corresponding bonding orbital. The total stabilization energy is therefore determined by the number of unoccupied d-orbitals (40) where h_j is the number of holes $(0, 1, 2)$ in the jth d orbital (corresponding to the number of electrons 2, 1, 0 respectively). In simple terms it is given by the destabilization energy of a particular

$$\Sigma(\sigma) = \beta_\sigma S_\sigma^2 \sum_j \ h_j \sum_i \ f_{ij}^2(\theta, \phi) \qquad (40)$$

d-orbital multiplied by the number of electron vacancies in that orbital, summed over all empty or half empty d-orbitals. Table 4 shows the stabilization energies from the three four-coordinate geometries of Fig. 12 as a func-
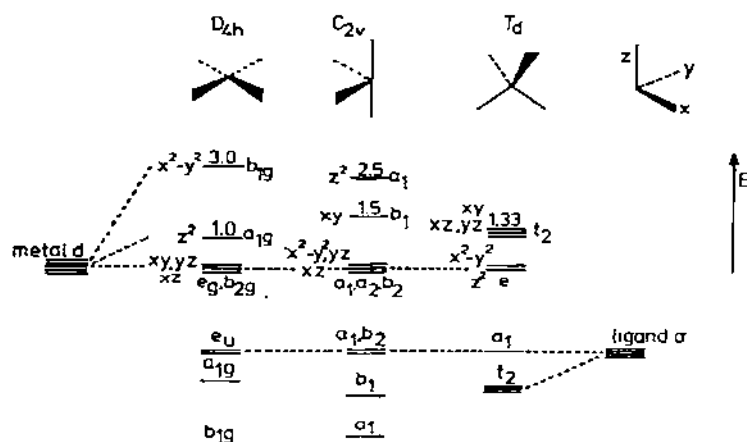
Fig. 12. Molecular orbital diagrams showing ligand σ—metal d orbital interactions in terms of the angular overlap model for square planar, octahedral cis divacant and tetrahedral geometries. The numbers showing the destabilization energies of the d-orbitals are in units of $\beta_\sigma S_\sigma^2$. We assume for simplicity here that the stabilization energy of a metal—ligand bonding orbital (mainly ligand located) is the same as the destabilization energy of the corresponding metal—ligand antibonding orbital (mainly metal located). Note the unconventional axis system for the C_{2v} structure. In some descriptions of the AOM the label e_σ is used in place of $\beta_\sigma S_\sigma^2$.

tion of d-orbital configuration. In the first column are the d-orbital occupation numbers — necessary to distinguish between high and low spin d^8 for example. For d^{10} Ni(CO)$_4$ with all the d-orbitals occupied there is no net stabilization energy from the d-orbital manifold for any geometry. (The molecule is held together by interaction of the ligand σ-orbitals with $(n + 1)$ s, p orbitals and by π back bonding of the filled d-shell with the carbonyl ligands.) For the other electronic configurations the geometries have different d-orbital stabilization energies. For the hs d^8 and ls d^6 systems two structures have equal values of $\Sigma(\sigma)$. If fourth-order terms are included in eqn. 36 then the general result emerges that the molecule with the larger number of cis ligands is the more stable [176].
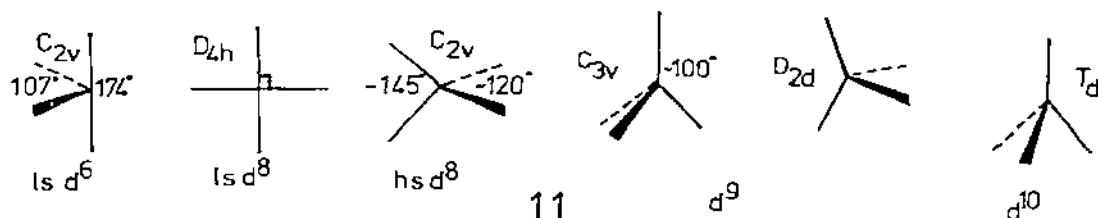
TABLE 4

d orbital stabilization energies for some four-coordinate structures (units $\beta_\sigma S_\sigma^2$)

d electron	Configuration	D_{4h}	T_d	C_{2v} [a]	Example
ls d^6	22200	8.0	5.3	8.0	Cr(CO)$_4$
ls d^8	22220	6.0	2.67	5.0	Ni(CN)$_4^{-2}$
hs d^8	22211	4.0	2.67	4.0	Fe(CO)$_4$
d^9	22221	3.0	1.33	2.5	Co(CO)$_4$
d^{10}	22222	0	0	0	Ni(CO)$_4$

[a] CMC angles 90° or 180°.

Before looking at these values in any detail it is pertinent to ask what would be the geometry of the molecule in the absence of the d-orbital electrons. With x σ-pairs the answer is the VSEPR structure, i.e. a trigonal plane for a three-coordinate and tetrahedron for a four-coordinate molecule etc. The shape of the molecule would be simply described by the rules applicable to main group complexes where the geometry is determined by the forces of interaction between s- and p-orbitals on the central atom and the ligand σ-orbitals. For d^{10} Ni(CO)$_4$ all the geometries of Table 4 have the same energy and thus there is no d-orbital driving force away from the tetrahedral geometry. This is the observed structure (11). For ls d^6 Cr(CO)$_4$ however the d-orbital driving force away from the tetrahedral geometry is substantial. The geometry observed is very close to the octahedral cis-divacant geometry demanded by the d-orbital manifold. For ls d^8 a similar large driving force sends four-coordinate molecules with this configuration to the square planar arrangement, (e.g. Ni(CN)$_4^{2-}$). For hs d^8 the driving force to the cis-divacant structure is smaller and insuffi-

cient to push the molecule all the way to the Cr(CO)$_4$ geometry. It has a structure described as distorted tetrahedral. The d^9 system also has a smaller driving force away from the tetrahedral geometry than does the ls d^8 system. The equilibrium geometry may therefore be somewhere along the D_{2d} coordinate. Interestingly for smallish distortions C_{3v} and D_{2d} structures compete for the lower energy geometry (i.e. the larger d-orbital driving force). The CuCl$_4^{2-}$ ion with this electronic configuration may be interconverted between the D_{2d} and D_{4h} geometries by the application of pressure [178]. Table 5 shows some data for three-coordinate species and similar arguments apply. Cr(CO)$_3$ has a larger destabilization of the trigonal planar geometry than Fe(CO)$_3$ and correspondingly has the more pronounced pyramidal structure.

The geometries of some of these structures may be approached by the use of the Jahn—Teller theorems. Thus four-coordinate ls d^6 or hs d^8 for example are Jahn—Teller unstable at the tetrahedral geometry and should distort. However, the theorem does not anticipate the pyramidal nature of Fe(CO)$_3$, which is well handled by the approach here. This molecule with a $^3A'_2$ electronic ground state at the D_{3h} geometry is not Jahn—Teller unstable. The second-. order Jahn—Teller approach does not work either if 'excitations' are restricted to within the d-orbital manifold. If higher energy excitations are allowed then all three tricarbonyls of Table 5 should be pyramidal which is clearly not the case [177]. Simple molecular orbital ideas then, although more complex than the rules of thumb of the VSEPR method, are well capable of rationalizing

TABLE 5

d orbital stabilization energies for some three-coordinate structures (units $\beta_\sigma S_\sigma^2$)

d electron	Configuration	C_{3v} [a]	D_{3h}	C_{2v} [b]	Example
ls d^6	22200	6.0	4.5	6.0	$Cr(CO)_3$
ls d^8	22220	3.0	2.25	4.73	
hs d^8	22211	3.0	2.25	3.0	$Fe(CO)_3$
d^9	22221	1.5	1.125	2.37	
d^{10}	22222	0	0	0	$Ni(CO)_3$

[a] CMC angles 90°. [b] CMC angles 90°, 180°.

the gross features of these structures. For more subtle effects we must naturally go to more sophisticated ideas.

F. THE UV AND VISIBLE PHOTOCHEMISTRY OF TRANSITION METAL CARBONYLS IN MATRICES

Some of the most studied carbonyls in low temperature matrices have been those of the Group VI metals, M = Cr, Mo and W. Photolysis of solutions containing $Cr(CO)_6$ in the presence of a ligand L lead to production of the Cr-$(CO)_5L$ species. Solution flash photolysis studies provide evidence for a short-lived intermediate which reacts with L to give product (41).

$$Cr(CO)_6 \xrightarrow{h\nu} Cr(CO)_5 \rightarrow Cr(CO)_5L \qquad (41)$$

The absorption maximum of the intermediate and its decay kinetics seemed to be very sensitive to the presence of impurities in the solvents used in such studies, a rather unusual result [179,180]. Photolytic studies of $M(CO)_6$ in various matrices confirmed the initial photolysis step in (41) but led to some other results which initially were very puzzling [181,182].

(i) A new carbonyl species, identified by CO isotope studies as C_{4v} $M(CO)_5$ was very readily produced on UV irradiation of the parent $M(CO)_6$, in spite of the cage restrictions on the position of the photoejected CO. On warming the matrix CO is very reluctant to recombine with $M(CO)_5$ [3].

(ii) On irradiation into the visible band of $M(CO)_5$ the parent carbonyl was efficiently generated by what overall is the rather unusual process of a photo-association reaction [3]. Such photochromic behavior (eqn. 6) has been shown to be typical of many matrix isolated systems.

(iii) The visible band of $M(CO)_5$ is incredibly sensitive to the nature of the matrix used [99]. Figure 13 shows the wavelength dependence of the band maximum on matrix material. These effects are too large to be ascribed to a solvent effect and are due to a specific interaction of the matrix with the pentacarbonyl as proved by (iv).

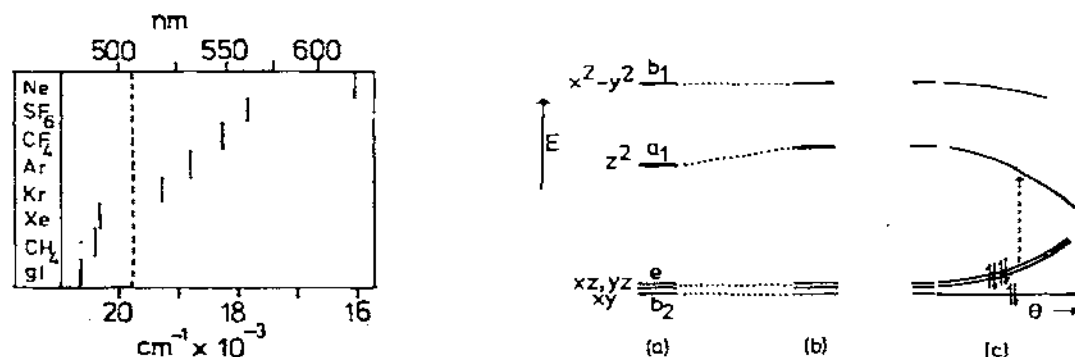(iv) By using a mixed matrix of Ne/Xe two visible bands were observed,

Fig. 13. Dependence of the visible absorption band maximum in Cr(CO)$_5$ on matrix material (gl = glass of methylcyclohexane/isopentane). The dotted line is the value found in solution flash photolysis.

Fig. 14. d orbital region of the molecular orbital diagram for (a) naked M(CO)$_5$; (b) with weak matrix interaction in the sixth site and (c) as a function of the axial/basal angle (θ). The visible absorption is represented as a transition from the e to a_1 orbital (dashed line).

one very close to that observed in pure Ne and one close to that observed in pure Xe. On visible photolysis of each of the Ne···M(CO)$_5$ (λ_1) and Xe···M-(CO)$_5$ (λ_2) bands the scheme 12 was observed. This is reminiscent of the solution photochemical reactions of W(CO)$_5$Pϕ_3 in the presence of another ligand L.
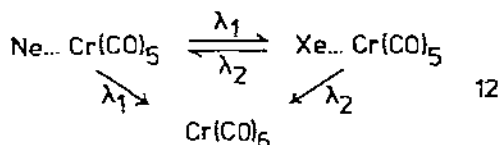

(v) Use of a polarised photolysis source and polarised UV/vis and IR detection of the products leads to another interesting observation [183]. The pentacarbonyl is rotated in the matrix on visible photolysis (13). (The actual
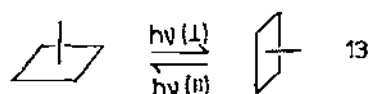
angle of rotation of the four-fold axis could, in principle, be determined by the rate of dichroic growth [185] but such measurements are very sensitive to errors.) Polarised photochemistry combined with polarised spectroscopic analysis of the products is a powerful tool when used to view processes occurring in low temperature matrices. The products of reaction are trapped and held rigidly in an orientation often related to the plane of polarisation of the incident photolysis radiation [186].

These observations may be rationalised in a very satisfactory way by con-

sidering in a little detail the electronic structure of the $M(CO)_5$ fragment itself. Figure 14 shows the d-orbital region of the molecular orbital diagram of a C_{4v} $M(CO)_5$ species. The visible electronic transition is almost certainly from the e-orbital to z^2. (Polarised spectroscopy on this matrix isolated species reveals [183] a transition moment of species e for the visible band which confirms the origin of the transition from the e pair of d-orbitals.) The z^2-orbital is located so that it points out of the bottom of the square pyramidal unit, ideally located for interaction with a two electron σ-donor. The donor may be CO (to give $M(CO)_6$) or the matrix itself to give matrix$\cdots M(CO)_5$. The latter interaction is of course smaller than the one with CO. The result of such interaction is to push z^2 to higher energy. This gives a partial explanation for the visible band shift in various matrices (Fig. 14b). A complementary factor is the energy change of z^2 and the xz, yz pair on bending (Fig. 14c). For Ar$\cdots$Cr $(CO)_5$ θ is $\sim 96°$ and for Xe$\cdots$Cr$(CO)_5$ it is $\sim 91°$ from the analysis of the IR intensities; i.e. the larger the sixth site occupant, the smaller is θ, and the higher energy the visible transition. These two effects combine to give a qualitative rationale for the data of Fig. 13 and the susceptibility of the absorption band in the flash experiments to impurities. The z^2-orbital in the $M(CO)_5$ unit is mixed with s and p_z and hybridised away from the axial CO ligand (14). It is therefore strongly metal—matrix antibonding when the matrix material is

14
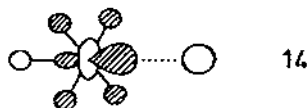
weakly coordinated in the sixth site. Excitation into z^2 therefore should lead to loss of the matrix molecule, leaving a truly 'naked' $M(CO)_5$ unit in an excited electronic state.

This state has a different electronic configuration (22110) to the ground state (22200) and may well have a different geometry. As we saw above the shapes of these transition metal carbonyls are very sensitive to the d-electron arrangement. AOM considerations, EHMO calculations and more sophisticated studies [171] point to a D_{3h} geometry for this excited state. A different geometry in the excited state compared to the electronic ground state allows the possibility of a photochemical intramolecular rearrangement process. It is one of these compatible with the geometry change, a reverse Berry process, which leads to an understanding of the $M(CO)_5$ photochemistry. Figure 15 shows the energy of the electronic ground state and electronic excited states as a function of the geometry change in the top half of 15. The tbp may decay to three possible C_{4v} geometries (a,b,c), each of which has a different arrangement of the four-fold axis in space. In the electronic ground state there is a sizeable barrier to interconversion of the various C_{4v} forms, aided no doubt by extra stabilization afforded by the matrix interaction. In the excited state this C_{4v} structure is now unstable with respect to the D_{3h} geometry where the ground and excited state potential curves touch. The pro-

cess of **15** then proceeds very smoothly as the system moves from top left to
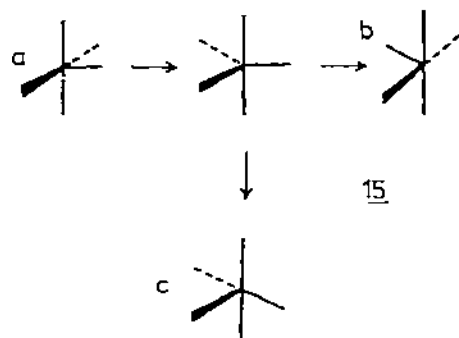
bottom right of Fig. 15, ending up with a ground state rearranged M(CO)₅ unit. On a molecular orbital basis the photochemical rearrangement is shown in Fig. 16.

This suggested rearrangement on visible photolysis allows explanation of all of the rest of the observations above. **15** is in fact a very similar diagram to the polarised photochemical result of **13** and immediately gives an explanation of this experimental result. Since the matrix environment probably remains rigid during photolysis (rather than some local 'soup') it provides a neat explanation of the mixed Ne/Xe experiment. If a rearrangement process
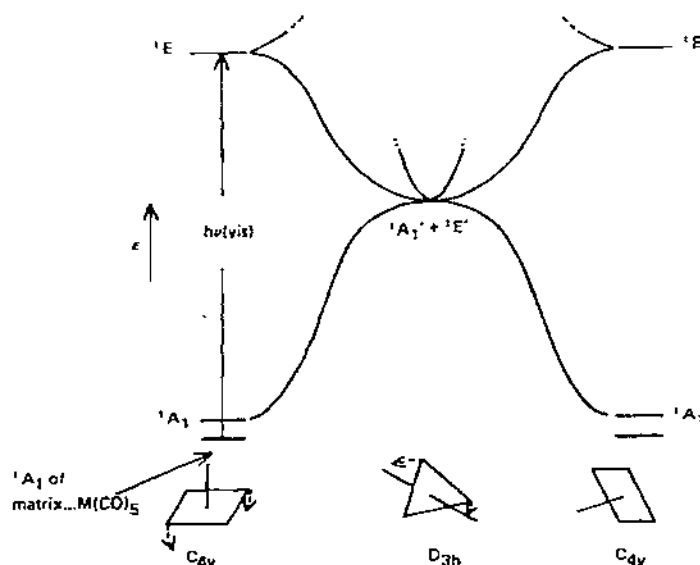
Fig. 15. The energies of the lowest energy singlet electronic states of d^6 M(CO)₅ as a function of the geometry change in the top half of **15**. The curves were computed using a one electron (EHMO) model, and thus electron—electron interactions which will split apart (e.g. E' and A_1' states of the tbp) are not included.
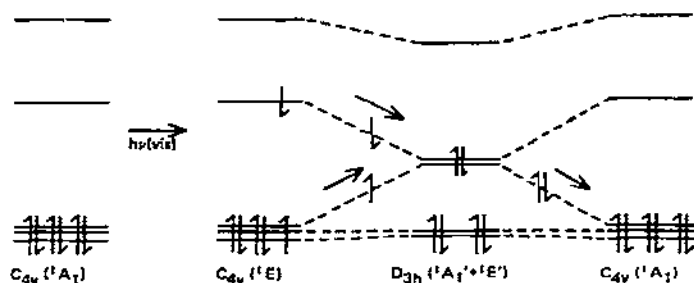
Fig. 16. The rearrangement process of Fig. 15 on a molecular orbital basis.

occurs with the initial UV photolysis of $M(CO)_6$ then the failure of CO to recombine instantly with the $M(CO)_5$ fragment and its reluctance to recombine on warming may also be understood. The ejected CO is not located adjacent to the sixth site after rearrangement. Studies using $trans\text{-}W(CO)_4(^{13}CO)$-(CS) confirm that such a rearrangement does in fact occur on initial UV photolysis as we will see below [16]. The overall photochemical scheme is shown in Fig. 17. A part of this scheme, although not its finer details was anticipated by Black and Braterman [187].

The photochromic behavior of eqn. 6 may be understood by tracing back along one visible photolysis pathway. On this scheme there is a 2 in 3 chance
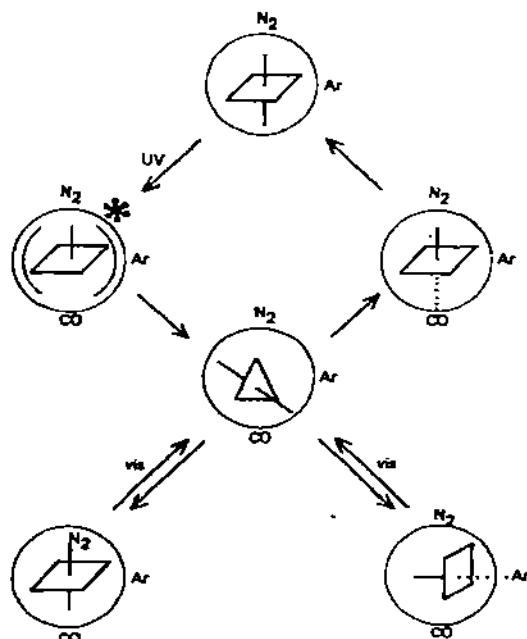

Fig. 17. A general scheme to rationalise the matrix photochemistry of d^6 $M(CO)_5$ molecules.

of forming an $M(CO)_5$ fragment on UV photolysis (we assume a quantum yield of 1 for breaking the M—CO bond) since one of the three arrangements of the C_{4v} unit contains the CO in the sixth site. Interestingly the quantum yield for photoproduction of all the Group VI pentacarbonyls in solution is 0.67 [188]. In addition each square pyramidal $M(CO)_5$ unit has a 1 in 6 chance of returning in one rearrangement step to the position where the CO is located in the sixth site ready for thermal recombination. (A 1 in 2 chance of moving to one particular tbp molecule and a 1 in 3 chance of moving from there to a particular spy structure). The ratio of quantum yields for the production ($\phi(vis)$) and reversal ($\phi(UV)$) reactions of eqn. 6 should then be 0.25. Experimentally in argon matrices the ratio $\phi(vis)/\phi(UV)$ is found to be 0.25 ± 0.05 [189]. Such agreement suggests that on receipt of a photon, each molecule makes only one traverse of the pathway in 15 although if more than one traverse occurred both $\phi(UV)$ and $\phi(vis)$ would decrease.

Polarised photochemical experiments with $Mo(CO)_5N_2$ in N_2 matrices [182] show that analogous behavior occurs with this species. Loss of N_2 occurs on near UV photolysis (into the equivalent of the visible band of $M(CO)_5$) followed by rearrangement of the $M(CO)_5$ and thermal recombination with N_2.

Whether photochemical rearrangements occur generally in transition metal carbonyl complexes is a sensitive function of electronic configuration. In solution $Mn_2(CO)_{10}$ readily photodissociates via a $\sigma \rightarrow \sigma^*$ excitation into two $Mn(CO)_5$ (ls d^7) species. In the matrix no $Mn(CO)_5$ is observed; after a long photolysis a small amount of CO loss is observed. Each $Mn(CO)_5$ produced by $\sigma \rightarrow \sigma^*$ excitation is in its electronic ground state of C_{4v} symmetry. No rearrangement occurs and the two species simply recombine (16). Another low
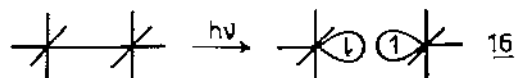
yield process explicable along similar lines is the photoproduction of $Ni(CO)_3$ from $Ni(CO)_4$ and the photodissociation reactions of d^{10} tetrahedral species in general. The $Ni(CO)_3$ cannot easily rearrange so as to change the orientation of an empty sp hybrid orbital and filled $d\pi$ type orbitals pointing out of the pyramidal unit and directly towards the relevant orbitals on the photoejected CO.

Another species of considerable interest from the point of view of its matrix photochemistry is $Fe(CO)_5$ [8,9,184]. The parent molecule $Fe(CO)_5$ is a singlet but $Fe(CO)_4$ and probably $Fe(CO)_3$ are triplets. Immediately the photochemical problem has become more complex since now both singlet and triplet manifolds need to be considered. Photochemical rearrangement processes certainly occur with $Fe(CO)_4$. Its reversal to $Fe(CO)_5$ takes place with the visible and NIR light of the Nernst glower of the IR spectrometer. A summary of some of the UV/vis photochemistry of $Fe(CO)_4$ is given in Fig. 18. Of interest is the production of the $Fe(CO)_4CH_4$ species which appears to be a trigonal bipyramid with the CH_4 in an equatorial site. This may be made
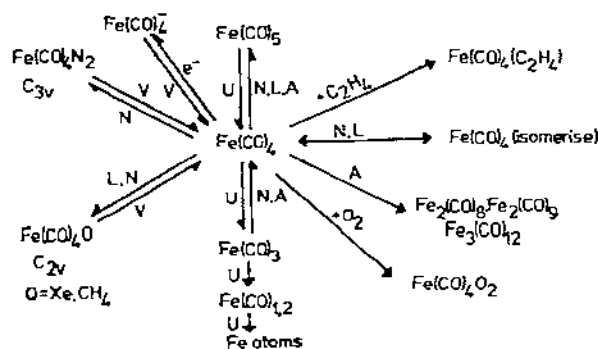
Fig. 18. A summary of the matrix reactions of Fe(CO)$_5$. Key: U = UV photolysis, N = Nernst glower or near IR photolysis. V = visible photolysis with a filtered Hg lamp such that $\lambda > 375$ nm, A = annealing, L = IR laser photolysis into the CO stretching bands of the molecule.

by visible photolysis of Fe(CO)$_4$ in solid methane or by the fascinating result of IR-laser irradiation into one of the CO stretching modes of Fe(CO)$_4$ [184].

It was mentioned above that on UV photolysis the W(CO)$_5$CS molecule rearranged in addition to losing CO. It is interesting to look at the experimental approach [16] to this problem since it illustrates a method which may be of general applicability in studying matrix isolated carbonyls and their reactions. On UV photolysis of W(CO)$_5$CS, on purely statistical grounds one might expect to observe a ratio of 4 : 1 of the C_s to C_{4v} isomers of W(CO)$_4$CS (17). In fact a ratio of 1 : 2 is observed signifying that either the axial CO
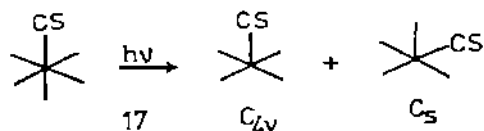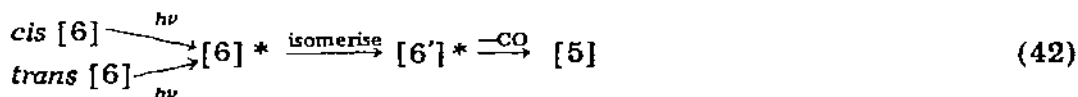

group *trans* to CS is preferentially labilised or that there is an excited state rearrangement of either the six- or five-coordinate unit. Experiments using *trans*-W(CO)$_4^{13}$CO CS excluded the preferential labilisation explanation (18).
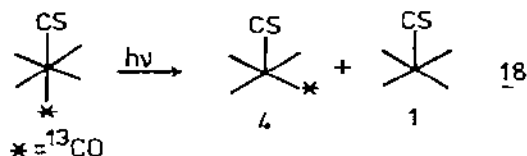
In order to get to the predominant product, the thiocarbonyl must lose an equatorial CO group and rearrange. This experiment does not distinguish, however, between isomerisation of the six-coordinate species before CO loss or rearrangement of the five-coordinate species after CO loss (42,43). By looking at the ratios of the photochemical products of the cis-labelled species (42)

could be excluded since photolysis of *cis* and *trans* molecules gave different

$$cis\ [6] \xrightarrow{h\nu} \atop trans\ [6] \xrightarrow{h\nu} [6]* \xrightarrow{\text{isomerise}} [6']* \xrightarrow{-CO} [5] \tag{42}$$

$$[6] \xrightarrow{h\nu} [6]* \rightarrow [5]* \xrightarrow{\text{isomerise}} [5'] \tag{43}$$

product distributions. The asterisk denotes an excited molecule. We suggested above that [5]* was probably the first excited singlet state of the molecule.
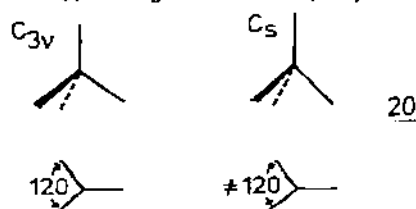
By the analysis of the product distribution of the photochemical reactions it is possible to eliminate some permutational descriptions of the rearrangement process and leave behind one consistent with a Berry-type process described in 15. Only a limited number of rearrangement events can occur, otherwise the product distribution would be a completely statistical one. The detailed description of how the excited matrix isolated molecule loses its energy to the matrix medium and how the rate of energy loss is related to the extent of rearrangement is a complex one which is scarcely understood. The ratio of the quantum yields $\phi(\text{vis})/\phi(\text{UV})$ for the photochromic process of eqn. 6 depends upon the matrix medium. In Ar it is 0.25 ± 0.05 but in CH_4 it is 0.04 ± 0.01 [189]. What limited evidence there is suggests that it is the reversal step which is much less efficient in the CH_4 matrix. This may be explicable perhaps by using the hypothesis that much more efficient matrix-molecule coupling occurs in the molecular CH_4 matrix compared to the monatomic Ar lattice, leading to less rearrangement in the CH_4 matrix. It is a field which only recently is beginning to be explored.

G. INFRA-RED PHOTOCHEMISTRY

This is a very new field in the realm of carbonyl chemistry and at the present time has only been illustrated with the $Fe(CO)_4$ molecule [11,175,184,190, 191]. Rearrangement induced with IR radiation is not new. *Cis—trans* isomerisation of matrix-isolated HONO was demonstrated several years ago [192]. In the $Fe(CO)_4$ case irradiation into the carbonyl stretching bands of the matrix isolated fragment with an IR laser led [184] to production of $Fe(CO)_4CH_4$ in a CH_4 matrix (Fig. 18). More specifically and dramatically, irradiation of a carbonyl stretching band of one of the possible isomers of isotopically labelled irreversible $Fe(CO)_4$ in an argon matrix (recall this does not reverse to $Fe(CO)_5$ on photolysis) led to conversion of one isomer to another in a very specific fashion (19) [175]. After a short irradiation into a single carbonyl stretching band a non-statistical distribution of isomers is produced. The statistical distribution may be regenerated by 'irradiation' with the Nernst-glower source of the IR spectrometer. With this radiation reversible $Fe(CO)_4$ could be reversed. This then proves that the reversal process involves a rearrangement of the $Fe(CO)_4$ unit and a permutational analysis of the rearrangement in 19 leads to a $h_3^{\nu w}$ process. This means that the transition state for the rearrangement may

$\star = {}^{13}C^{18}O$ 19
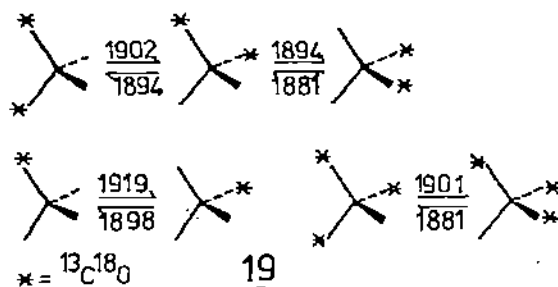
not be T_d, C_{4v}, D_{4h} or any structure where all four CO groups are equivalent. A C_{3v} or C_s structure (20) is consistent with this permutational exchange. Inter-

estingly, structures with these geometries are calculated to be very close (<0.7 kcal (~3 kJ) mole^{-1}) in energy to the C_{2v} ground state [193]. This exchange process 19 where one 'axial' and one 'equatorial' group is exchanged is opposite to the one found for the structurally similar SF_4 molecule [194]. Here both axial groups exchange with both equatorial groups in one step. Of considerable chemical interest is that when $Fe(CO)_4$ is irradiated in the IR in CH_4 matrices, $Fe(CO)_4CH_4$ is readily formed [184] but in N_2 matrices isomerisation without reaction with the N_2 occurs [190]. Both species may be made by conventional electronic excitation [9].

The IR photolysis is a single photon process from yield studies over a wide range of incident powers [11]. The laser photon energy of ~2000 cm^{-1} ≃ 5.5 kcal mole^{-1} is sufficient to reach the calculated energy of the transition state. The resultant energy transfer process from a carbonyl stretching coordinate to the deformation coordinate involved in the angular distortion of the C_{2v} structure will surely be an interesting one to study. The IR laser photolysis method may well turn out to be a valuable tool in studying thermal rearrangements (at 20 K!) of these carbonyl fragments in matrices. Its major drawback is the restriction of ~5.5 kcal mole^{-1} as the highest energy of activation that is accessible with the 2000 cm^{-1} photon. There is a possibility of irradiating overtones and combination bands at twice this energy but the absorptions are not particularly intense. An alternative might be to increase laser powers and induce multi-photon processes.

H. CARBONYL ANIONS IN MATRICES

Several matrix studies exist of charged main group species such as $B_2H_6^-$ and CCl_3^- but only a few of transition metal carbonyl ions. These species have been

made in low temperature matrices in three ways [5,68,103].

(i) Cocondensation of a stable metal carbonyl with sodium and subsequent visible photolysis (44).

$$Na \xrightarrow{h\nu} Na^+ + e^-$$

$$e^- + Cr(CO)_6 \rightarrow [Cr(CO)_6^-] \rightarrow Cr(CO)_5^- + CO \tag{44}$$
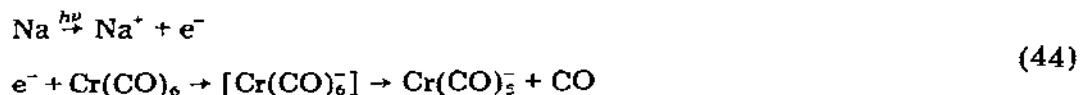
The alkali metal acts as an electron source and $Cr(CO)_5^-$ (a 17-electron species) is most probably formed by dissociative electron capture, via the 19-electron species $Cr(CO)_6^-$. In fact some cooperative coupling between the two steps of (44) occurs since the frequency of visible light used is less than that needed to ionise sodium. (A similar observation was noted [195] in the production of pyridyl$^-$ by the same method.) The photoejected CO molecule probably lies close to the $Cr(CO)_5^-$ unit since the IR spectrum of the ion is considerably split.

(ii) Vacuum UV irradiation of the matrix. High energy irradiation of the trapped carbonyl in this region provides enough energy to ionise the molecule. These photoelectrons may react with other carbonyl molecules as in (44). The source of photoelectrons need not be the species deliberately matrix isolated. On VUV production of NO_2^- from NO_2 no absorptions were observed from NO_2^+ suggesting that the photoelectrons came from impurities (water, hydrocarbon grease) in the matrix [196]. In all VUV experiments with metal carbonyls bands are observed also at high frequency and are due to $M(CO)_y^+$. Since the extinction coefficient of $\nu(CO)$ bands increases with decreasing frequency the structural characterization by isotopic substitution of the species responsible for these high frequency, low intensity bands has not proved possible.

(iii) High energy particle bombardment. Another way of ionising molecules in matrices to produce electrons is to bombard the carbonyl species with high energy particles. 500 eV electrons have been particularly effective when used during slow spray-on of $Ar/M(CO)_y$ mixtures. In these experiments bands due to carbonyl anions and cations have been observed [68].

It is interesting that with all 18-electron carbonyls studied, $Cr(CO)_6$, Fe-$(CO)_5$ and $Ni(CO)_4$, CO loss occurs on electron capture to avoid the formation of 19-electron species. The anion and ejected CO share the same matrix cage and their recombination prevented due to the spontaneously dissociative nature of the parent anion. Some of these ions have also been observed using Ion Cyclotron Resonance in the gas phase. Here also no 19-electron species was detected [197,198]. With the 17-electron carbonyl $V(CO)_6$ the extra electron is captured without CO loss and the 18-electron $V(CO)_6^-$ is produced. (This species is of course known under 'normal conditions'.) For these carbonyl molecules the energetic demands of the 18-electron rule seems to be strong indeed. Interestingly $Fe(CO)_4^-$ is non-tetrahedral, showing that the distorted structure observed for this species in the matrix is not induced by the medium.

I. STUDIES ON STABLE CARBONYLS

Most studies on stable carbonyls in matrices have taken advantage of the rigidity imposed on the species when trapped at these low temperatures and also on the sharp IR bands usually found in these media. Thus recently a third isomer of $Co_2(CO)_8$ was identified [199] by a careful study of the IR spectrum of a matrix isolated sample and the temperature dependence of the intensities of groups of bands. The suggested structure of the third isomer is shown in 21


21
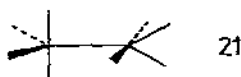
and its relationship to the other two isomers has been studied by molecular-orbital calculations. The matrix method succeeded in splitting apart bands which would not have been resolved in the solution spectrum.

The low temperature matrix usually traps molecules in random orientations with respect to a set of laboratory fixed axes, and here each molecule remains frozen in one particular orientation. However if the molecules are photolysed with polarised light then the probability of photolysis will depend upon the orientation of the molecule with respect to the plane of polarisation of the photolysis radiation. Left behind after the photochemistry are molecules with non-random orientations in the matrix. This partially ordered sample now possesses dichroic properties, i.e. the intensities of bands in the electronic and vibrational spectra will depend upon the orientation of the plane of polarisation of the sampling radiation. The polarisation properties allow determination of the symmetry species of the transition moment for a particular transition. For example the 352 nm absorption in $Mo(CO)_5N_2$ was shown [182] to be of the same symmetry species as the e $\nu(CO)$ stretching vibration. Polarised photochemical studies by Turner and co-workers on $Fe(CO)_5$ allowed similar confirmation of the assignment of electronic spectral bands and also showed that the molecule was not fluxional at 20 K [201]. $Fe(CO)_5$ was isolated in pure CO at 20 K and photolysed with polarised UV radiation at 255 nm. Under these conditions $Fe(CO)_5$ loses CO to give $Fe(CO)_4$. However, because of the large CO concentration very little $Fe(CO)_4$ is actually observed; most of it combines with the matrix to reform parent. The effect of the polarised photolysis is to 'burn away' $Fe(CO)_5$ molecules in particular orientations where they have a high absorption probability and send them to other less vulnerable positions. This leaves a dichroic sample. One very interesting point about the experiment is that the dichroism did not decay with time, showing that the molecule is not fluxional under these conditions. (Similar comments apply to $Cr(CO)_5$ studied in a similar way [183].) It had previously been claimed [202] that $Fe(CO)_5$ was fluxional at 4 K in the solid. From the polarised matrix experiment an upper limit of 10^{-4} Hz could be put on the fluxional frequency.

J. RELEVANCE OF MATRIX ISOLATION STUDIES TO CATALYTIC PROCESSES

In previous sections we noted the observation of infra-red bands due to $M_{cl}CO$ or $M_{cl}N_2$ which may be produced by evaporation of quantities of metal atoms into a low temperature matrix. However some of the mononuclear species characterized in low temperature matrices may also be good models for viewing heterogeneous catalytic processes. For example Table 6 shows the IR frequencies of gaseous ethylene, ethylene adsorbed on Pd (Pd $(C_2H_4$, ads)) from conventional studies and the frequencies of the molecule $Pd(C_2H_4)$ made by Ozin and co-workers [136]. The similarity between the second and third numbers for the chemically sensitive C=C stretching mode is striking and suggests perhaps that the effect on the ethylene structure is not very sensitive to the number of coordinating metal atoms. More recently, under carefully controlled conditions, the molecule $Ni_2(C_2H_4)$ has been prepared and its UV/vis and IR spectra are very similar in quantitative terms to those of $Ni(C_2H_4)$ itself [41].

It is of somewhat greater interest however to try and observe under matrix conditions various intermediates and steps in a chemical process which is catalysed by metals in a more conventional environment. This has recently been done [203]. Silver acts as a heterogeneous oxidation catalyst for ethylene and leads very selectively to ethylene oxide. In low temperature matrices which have been made by cocondensation of $O_2/C_2H_4/Ar$ and Ag atoms the species AgO_2, $Ag(C_2H_4)$ and $Ag(C_2H_4)O_2$ may be identified. On warming this matrix to 30 K bands due to the first two species decrease in intensity and new bands tentatively assigned to the species 22 are observed. This is a species
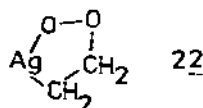
very similar to the one proposed in the real catalytic system. The major problem associated with this experiment is the difficulty of structurally characterizing 22 by the use of IR and Raman and isotopic techniques.

The cocondensation of $CO/O_2/Ar$ with silver atoms leads to the species $[OCAg^+]O_2^-$ which decomposes at about 40 K without production of CO_2.

TABLE 6

Absorption bands of C_2H_4 (cm^{-1})

Mode	(C_2H_4) gas	$Pd(C_2H_4)$	$Pd(C_2H_4)$ ads
νCH_2	2986	2952	2980
$\nu(C=C)$	1623	1502	1510
$\delta(CH_2)$	1443	1223	not obs.
$\rho(CH_2)$	949	913	not obs.

With Au atoms a very different set of species is produced and reactions occur. Firstly two $\nu(CO)$ bands are observed at high frequency and another in the ketonic region. Isotope experiments with $^{12}C^{16}O$, $^{13}C^{18}O$, $^{16}O_2$, $^{16}O^{18}O$ and $^{18}O_2$ produced spectra that were consistent with a peroxyformate structure 23. At 40 K this complex breaks down to give CO_2. The spectral changes
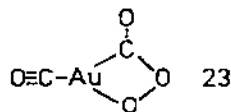
and their isotopic dependence indicate a two step process for the loss of two CO_2 molecules (24). The extension of the model process to that occurring on
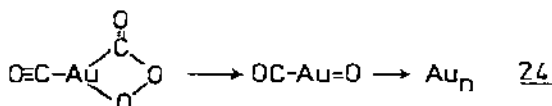
a gold surface is clear, if the CO and O_2 absorb at the same site. If the ligands absorb at different sites then the model complex only partially describes the reaction pathway. In any case experiments like these are full of promise for the future where it may be possible to study such processes which are difficult to tackle using other approaches.

ACKNOWLEDGEMENTS

REFERENCES

1 For two excellent review articles see Specialist Periodic Reports of the Chemical Society Molecular Spectroscopy. A.J. Downs and S.C. Peake, 1 (1973) 523 and B.M. Chadwick 3 (1975) 281.
2 J.J. Turner, Angew. Chem. (Int. Ed. Engl.), 14 (1975) 304.
3 M.A. Graham, M. Poliakoff and J.J. Turner, J. Chem. Soc. (A), (1971) 2939.
4 R.N. Perutz and J.J. Turner, J. Chem. Soc. Faraday Trans. 2, 69 (1973) 452.
5 J.K. Burdett, Chem. Commun., (1973) 763.
6 A.J. Rest, J. Organometal. Chem., 40 (1972) C76.
7 G.A. Ozin and A. Van der Voet, Can. J. Chem., 51 (1973) 3332.
8 M. Poliakoff and J.J. Turner, J. Chem. Soc. Dalton Trans. (1973) 1351.
9 M. Poliakoff and J.J. Turner, J. Chem. Soc. Dalton Trans. (1974) 2276.
10 M. Poliakoff, J. Chem. Soc. Dalton Trans. (1974) 210.
11 M. Poliakoff, B. Davies, A. McNeish, M. Tranquille and J.J. Turner, Ber. Bunsenges. Ges., 82 (1978) 127.
12 M. Poliakoff and J.J. Turner, J. Chem. Soc. Faraday Trans. 2, 70 (1974) 93.

13 J.K. Burdett and J.J. Turner in G.A. Ozin and M. Moskovits (Eds.), Cryogenic Chemistry, Wiley, New York, 1976.
14 D.E. Milligan and M.E. Jacox, J. Chem. Phys., 47 (1967) 278.
15 R.N. Perutz, Ph.D. Thesis, University of Cambridge, 1974.
16 M. Poliakoff, Inorg. Chem., 15 (1976) 2892.
17 M. Moskovits and G.A. Ozin, J. Mol. Struct., 32 (1976) 71.
18 E.P. Kundig, M. Moskovits and G.A. Ozin, Angew. Chem. (Int. Ed. Engl.), 14 (1975) 292.
19 P.L. Timms, Advan. Inorg. Chem. Radiochem., 14 (1972) 121.
20 K.J. Klabunde, Accounts Chem. Res., 8 (1975) 383.
21 V.M. Akhmedov, M.T. Anthony, M.L.H. Green and D. Young, J. Chem. Soc. Dalton Trans., (1975) 1412.
22 E. Koerner von Gustorf, O. Jaenicke and O.E. Polansky, Angew. Chem. (Int. Ed. Engl.), 77 (1972) 532.
23 G.A. Ozin and A. Van der Voet, Accounts Chem. Res., 6 (1973) 313.
24 H. Huber, M. Moskovits and G.A. Ozin, Nature (Phys. Sci.), 236 (1972) 127.
25 H. Huber, M. Moskovits and G.A. Ozin, Nature (Phys. Sci.), 239 (1972) 48.
26 M. Moskovits and G.A. Ozin, Appl. Spectrosc., 26 (1972) 481.
27 H. Huber, E.P. Kundig, G.A. Ozin and A.J. Poe, J. Am. Chem. Soc., 97 (1975) 308.
28 T.C. DeVore, A. Ewing, H.F. Franzen and V. Calder, Chem. Phys. Lett., 35 (1975) 78.
29 J.E. Hulse and M. Moskovits, J. Chem. Phys., 66 (1977) 3988.
30 R. Busby, W. Klotzbucher and G.A. Ozin, J. Am. Chem. Soc., 98 (1976) 4013.
31 E.P. Kundig, M. Moskovits and G.A. Ozin, Nature (Phys. Sci), 254 (1975) 503.
32 W. Klotzbucher and G.A. Ozin, Inorg. Chem., 16 (1977) 984.
33 H. Huber, E.P. Kundig, M. Moskovits and G.A. Ozin, J. Am. Chem. Soc., 97 (1975) 2097.
34 A.J. Hinchcliffe, J.S. Ogden and D.D. Oswald, Chem. Commun., (1972) 338.
35 R.F. Turner, Ph.D. Thesis, University of Newcastle upon Tyne, 1976.
36 M.A. Graham, Ph.D. Thesis, University of Cambridge, 1971.
37 R.L. DeKock, Inorg. Chem., 10 (1971) 1205.
38 J.K. Burdett and J.J. Turner, Chem. Commun., (1971) 885.
39 J.K. Burdett, M.A. Graham and J.J. Turner, J. Chem. Soc. Dalton Trans., (1972) 1620.
40 R.P. Eischens and J. Jacknow, Proc. Int. Cong. on Catalysis, Amsterdam, 1965, Vol. 1, p. 627.
41 W.J. Power, G.A. Ozin, W.A. Goddard and T.H. Upton, J. Am. Chem. Soc., 100 (1978) in press; G.A. Ozin and W.J. Power, Ber. Bunsenges. Ges., (1978) in press.
42 I.W. Stolz, G.R. Dobson and R.K. Sheline, J. Am. Chem. Soc., 84 (1962) 3589; 85 (1963) 1013.
43 J.D. Black, M.J. Boylan, P.S. Braterman and W.J. Wallace, J. Organometal. Chem., 63 (1973) C21.
44 J.D. Black and P.S. Braterman, J. Organometal. Chem. 63 (1973) C19.
45 J.D. Black and P.S. Braterman, J. Organometal. Chem., 85 (1975) C7.
46 J.D. Black, Ph.D. Thesis, University of Glasgow, 1975.
47 K.J. Klabunde, Angew. Chem. (Int. Ed. Engl.), 14 (1975) 287.
48 A.G. Massey and L.E. Orgel, Nature, 191 (1961) 1386.
49 J.K. Burdett, H. Dubost, M. Poliakoff and J.J. Turner in R.J.H. Clark and R.E. Hester (Eds.), Advances in Infra-red and Raman Spectroscopy, Vol. II , Heyden, London, 1976.
50 O. Crichton and A.J. Rest, Inorg. Nucl. Chem. Lett., 9 (1972) 391.
51 J.H. Darling and J.S. Ogden, J. Chem. Soc. Dalton Trans., (1972) 2496.
52 E.P. Kundig and G.A. Ozin, J. Am. Chem. Soc., 96 (1974) 3820.
53 R.N. Perutz and J.J. Turner, Inorg. Chem., 14 (1975) 262.
54 J.K. Burdett, M.A. Graham, R.N. Perutz, M. Poliakoff, A.J. Rest, J.J. Turner and R.F. Turner, J. Am. Chem. Soc., 97 (1975) 4805.
55 L.H. Jones, R.S. McDowell and M. Goldblatt, Inorg. Chem., 8 (1969) 2349.

56 L.H. Jones, R.S. McDowell and B.I. Swanson, J. Chem. Phys., 58 (1973) 3757.
57 L.H. Jones, R.S. McDowell and M. Goldblatt, J. Chem. Phys., 48 (1968) 2663.
58 D.K. Ottensen, H.B. Gray, L.H. Jones and M. Goldblatt, Inorg. Chem., 12 (1973) 1050.
59 F.A. Cotton and C.S. Kraihanzel, J. Am. Chem. Soc., 84 (1962) 4432.
60 C.S. Kraihanzel and F.A. Cotton, Inorg. Chem., 2 (1963) 533.
61 F.A. Cotton, Inorg. Chem., 3 (1964) 702.
62 P.S. Braterman, Metal Carbonyl Spectra, Academic Press, New York, 1975.
63 L.H. Jones in S. Kirschner (Ed.), Advances in the Chemistry of the Coordination Compounds, Macmillan, New York, 1961.
64 J.K. Burdett, M. Poliakoff, J.A. Timney and J.J. Turner, Inorg. Chem., 17 (1978) 948.
65 M. Bigorgne, Spectrochim. Acta Part A, 31 (1975) 1151; 32 (1976) 673.
66 J.K. Burdett, R.N. Perutz, M. Poliakoff and J.J. Turner, Inorg. Chem., 15 (1976) 1245.
67 G. Bor, Inorg. Chim. Acta, 3 (1969) 191.
68 P.A. Breeze, J.K. Burdett and J.J. Turner, Inorg. Chem., 17 (1978) in press.
69 H. Haas and R.K. Sheline, J. Chem. Phys., 47 (1967) 2996.
70 P.S. Braterman, R. Bau and H.D. Kaesz, Inorg. Chem., 6 (1967) 2097.
71 E.W. Abel and I.S. Butler, Trans. Faraday Soc., 63 (1967) 45.
72 L.M. Haines and M.H.B. Stiddard, Advan. Inorg. Chem. Radiochem., 12 (1970) 53.
73 S.F.A. Kettle and I. Paul, Advan. Organometal. Chem., 10 (1972) 199.
74 T.L. Brown and D.J. Darensbourg, Inorg. Chem., 6 (1967) 971.
75 D.J. Darensbourg and T.L. Brown, Inorg. Chem., 7 (1968) 959.
76 A.R. Manning and J.R. Miller, J. Chem. Soc. (A), (1966) 1521.
77 R.N. Perutz and J.J. Turner, J. Am. Chem. Soc., 91 (1975) 4800
78 J.K. Burdett and J.J. Turner, to be published.
79 M. Poliakoff, Inorg. Chem., 15 (1976) 2022.
80 J.R. Miller, J. Chem. Soc. (A), (1971) 1885.
81 D. Tevault and K. Nakamoto, Inorg. Chem., 14 (1975) 2371.
82 A.D. Cormier, J.D. Brown and K. Nakamoto, Inorg. Chem., 12 (1973) 3011.
83 J.A. Timney, to be published.
84 I.S. Butler and D.A. Johansson, Inorg. Chem., 14 (1975) 701.
85 J.K. Burdett, A.J. Downs, G.P. Gaskill, M.A. Graham and J.J. Turner, Inorg. Chem., 17 (1978) 523.
86 D.J. Darensbourg, H.H. Nelson and C.L. Hyde, Inorg. Chem., 13 (1974) 2135.
87 G.A. Ozin and A. Van der Voet, Can. J. Chem., 51 (1973) 637.
88 W.E. Klotzbucher and G.A. Ozin, J. Am. Chem. Soc., 95 (1973) 3790.
89 D. McIntosh and G.A. Ozin, Inorg. Chem., 16 (1977) 51.
90 D.R. Bevis, Pt. II Thesis, University of Oxford, 1974.
91 H. Huber, W. Klotzbucher, G.A. Ozin and A. Van der Voet, Can. J. Chem., 51 (1973) 2722.
92 H. Huber and G.A. Ozin, Can. J. Chem., 50 (1972) 3746.
93 R. Busby, W. Klotzbucher and G.A. Ozin, Inorg. Chem., 16 (1977) 822.
94 L. Hanlan, H. Huber and G.A. Ozin, Inorg. Chem., 15 (1976) 2592.
95 G.A. Ozin and A. Van der Voet, Progr. Inorg. Chem., 19 (1975) 105.
96 T.A. Ford, H. Huber, W. Klotzbucher, M. Moskovits and G.A. Ozin, Inorg. Chem., 15 (1976) 1666.
97 T.C. DeVore and H.F. Franzen, Inorg. Chem., 15 (1976) 1318.
98 H. Huber, T.A. Ford, W. Klotzbucher and G.A. Ozin, J. Am. Chem. Soc., 98 (1976) 3176.
99 R.N. Perutz and J.J. Turner, J. Am. Chem. Soc., 97 (1975) 4791.
100 M.A. Graham, R.N. Perutz, M. Poliakoff and J.J. Turner, J. Organometal. Chem., 34 (1972) C34.
101 M.A. Graham, A.J. Rest and J.J. Turner, J. Organometal. Chem., 24 (1970) C54.
102 A.J. Rest and J.R. Sodeau, Chem. Commun., (1975) 696.
103 P.A. Breeze and J.J. Turner, J. Organometal. Chem., 44 (1972) C7.

56

104 T.C. DeVore, Inorg. Chem., 15 (1976) 1315.
105 J.H. Darling, M.B. Garton-Sprenger and J.S. Ogden, Faraday Symp. Chem. Soc., 8 (1973) 75.
106 A.J. Rest and J.J. Turner, Chem. Commun., (1969) 375.
107 J.F. Olgivie, Chem. Commun., (1970) 323.
108 A.J. Rest, Chem. Commun., (1970) 345.
109 T.J. Barton, R. Grinter, A.J. Thomson, B. Davies and M. Poliakoff, Chem. Commun. (1977) 841.
110 B.I. Swanson, L.H. Jones and R.R. Ryan, J. Mol. Spectrosc., 45 (1973) 324.
111 O.L. Chapman, J. Pacansky and P.W. Wojtkowski, Chem. Commun., (1973) 681.
112 M.J. Newlands and J.F. Olgivie, Can. J. Chem., 49 (1971) 343.
113 A.J. Rest, J. Organometal. Chem., 40 (1972) C76.
114 O. Crichton and A.J. Rest, J. Chem. Soc. Dalton Trans., (1977) 656.
115 M. Poliakoff and J.J. Turner, J. Chem. Soc. (A), (1971) 2403.
116 M. Poliakoff and J.J. Turner, J. Chem. Soc. (A), (1971) 654.
117 M. Poliakoff and J.J. Turner, Chem. Commun., (1970) 1008.
118 P.H. Barrett and P.A. Montano, J. Chem. Soc. Faraday Trans. 2, 73 (1977) 378.
119 O. Crichton, M. Poliakoff, A.J. Rest and J.J. Turner, J. Chem. Soc. Dalton Trans., (1973) 1321.
120 L. Hanlan, H. Huber, E.P. Kundig, B.R. McGarvey and G.A. Ozin, J. Am. Chem. Soc 97 (1975) 7054.
121 H. Huber, E.P. Kundig and G.A. Ozin. J. Am. Chem. Soc., 96 (1974) 5585.
122 G.A. Ozin in H.E. Hallam (Ed.), Vibrational Spectroscopy of Trapped Species, Wiley New York, 1973.
123 L.A. Hanlan and G.A. Ozin, J. Am. Chem. Soc., 96 (1974) 6324.
124 A.J. Rest and J.J. Turner, Chem. Commun., (1969) 1026.
125 A.J. Rest and D.J. Taylor, Chem. Commun., (1977) 717.
126 E.P. Kundig, M. Moskovits and G.A. Ozin, J. Mol. Struct., 14 (1972) 137.
127 H. Huber, E.P. Kundig, M. Moskovits and G.A. Ozin, J. Am. Chem. Soc., 95 (1973) 332.
128 D.A. Van Liersburg and C.W. DeKock, J. Phys. Chem., 78 (1974) 134.
129 D.A. Van Liersburg and C.W. DeKock, J. Am. Chem. Soc., 94 (1972) 3255.
130 H. Huber, G.A. Ozin and W.J. Power, Inorg. Chem., 16 (1977) 2234.
131 E.P. Kundig, M. Moskovits and G.A. Ozin, Can. J. Chem., 51 (1973) 2737.
132 H. Huber, G.A. Ozin and W.J. Power, J. Am. Chem. Soc., 98 (1976) 6508.
133 E.P. Kundig, M. Moskovits and G.A. Ozin, Can. J. Chem., 50 (1972) 3587.
134 J.H. Darling and J.S. Ogden, Inorg. Chem., 11 (1972) 666.
135 G.A. Ozin, M. Moskovits, P. Kundig and H. Huber, Can. J. Chem., 50 (1972) 2385.
136 H. Huber, G.A. Ozin and W.J. Power, Inorg. Chem., 16 (1977) 979.
137 G.A. Ozin and W.J. Power, Inorg. Chem., 16 (1977) 212.
138 O. Crichton and A.J. Rest, Chem. Commun., (1973) 407.
139 O. Crichton and A.J. Rest, J. Chem. Soc. Dalton Trans., (1977) 986.
140 G. Blyholder, M. Tanaka and J.D. Richardson, Chem. Commun., (1971) 499.
141 D. McIntosh, E.P. Kundig, M. Moskovits and G.A. Ozin, J. Am. Chem. Soc., 95 (1973) 7234.
142 D.W. Green, J. Thomas and D.M. Gruen, J. Chem. Phys., 58 (1973) 5453.
143 E.P. Kundig, M. Moskovits and G.A. Ozin, Can. J. Chem., 51 (1973) 2710.
144 H. Huber, E.P. Kundig, M. Moskovits and G.A. Ozin, J. Am. Chem. Soc., 97 (1975) 2097.
145 J.S. Ogden, Chem. Commun., (1971) 978.
146 P.H. Kasai and D. McLeod, Jr., J. Am. Chem. Soc., 100 (1978) 625.
147 D. McIntosh and G.A. Ozin, J. Am. Chem. Soc., 98 (1976) 3167.
148 D. McIntosh, M. Moskovits and G.A. Ozin, Inorg. Chem., 15 (1976) 1669.
149 D. McIntosh and G.A. Ozin, Inorg. Chem., 16 (1977) 59.

150 H. Huber and G.A. Ozin, Inorg. Chem., 16 (1977) 64.
151 D. McIntosh and G.A. Ozin, Inorg. Chem., 15 (1976) 2869.
152 H. Huber, D. McIntosh and G.A. Ozin, Inorg. Chem., 16 (1977) 975.
153 D. McIntosh and G.A. Ozin, J. Organometal. Chem., 121 (1976) 127.
154 H. Huber, D. McIntosh and G.A. Ozin, J. Organometal. Chem., 112 (1976) C50.
155 J.L. Slater, T.C. DeVore and V. Calder, Inorg. Chem., 13 (1974) 1808.
156 J.L. Slater, T.C. DeVore and V. Calder, Inorg. Chem., 12 (1973) 1918.
157 J.L. Slater, R.K. Sheline, K.C. Lin and W. Weltner, J. Chem. Phys., 55 (1971) 5129.
158 P.H. Kasai, D. McLeod and T. Watanabe, J. Am. Chem. Soc., 99 (1977) 3521.
159 A. Bos. Chem. Commun., (1972) 26.
160 M.A. Hooper and A.J. Downs, (unpublished).
161 D. Tevault and K. Nakamoto, Inorg. Chem., 15 (1976) 1282.
162 R.J. Gillespie, Molecular Geometry, Van Nostrand-Rheinhold, New York 1972.
163 R.J. Gillespie and R.S. Nyholm, Quart. Rev., 11 (1957) 339.
164 A.B.P. Lever and G.A. Ozin, Inorg. Chem., 16 (1977) 2012.
165 R.R. Gagne, J.L. Allison, R.S. Gall and C.A. Kaval, J. Am. Chem. Soc., 100 (1978) in press.
166 P.S. Braterman, Struct. Bonding, 10 (1972) 57.
167 P.S. Braterman, Struct. Bonding, 26 (1976) 1.
168 O. Crichton, Ph. D. Thesis, University of Cambridge, 1975.
169 J.R. Sodeau, Ph.D. Thesis, University of Southampton, 1976.
170 J. Demuynck, A. Strick and A. Veillard, Nouv. J. Chim., 1 (1977) 217.
171 P.J. Hay, J. Am. Chem. Soc., 100 (1978) 2411.
172 I.H. Hillier and V.R. Saunders, Chem. Commun., (1971) 642.
173 J.K. Burdett, J. Chem. Soc. Faraday Trans. 2, 70 (1974) 1599.
174 M. Elian and R. Hoffmann, Inorg. Chem., 14 (1975) 1058.
175 B. Davies, A. McNeish, M. Poliakoff and J.J. Turner, J. Am. Chem. Soc., 99 (1977) 7573.
176 J.K. Burdett, Inorg. Chem., 14 (1975) 375.
177 J.K. Burdett, Advan. Inorg. Chem. Radiochem., 21 (1978) 113.
178 J.R. Ferraro and J. Long, Accounts Chem. Res., 8 (1975) 171.
179 J.M. Kelly, H. Herman and E.A. Koerner von Gustorf, Chem. Commun., (1973) 105.
180 J.M. Kelly, D.W. Best, H. Hermann, D. Schulte-Fröhlinde and E.A. Koerner von Gustorf, J. Organometal. Chem., 69 (1974) 259.
181 J.J. Turner, J.K. Burdett, R.N. Perutz and M. Poliakoff, Pure Appl. Chem., 49 (1977) 271.
182 J.K. Burdett, J.M. Grzybowski, R.N. Perutz, M. Poliakoff, J.J. Turner and R.F. Turner, Inorg. Chem., 17 (1978) 147.
183 J.K. Burdett, R.N. Perutz, M. Poliakoff and J.J. Turner, Chem. Commun., (1975) 157.
184 A. McNeish, M. Poliakoff, K.P. Smith and J.J. Turner, Chem. Commun., (1976) 859.
185 J.K. Burdett and I.R. Dunkin, unpublished work.
186 J.K. Burdett, I.R. Dunkin, J.M. Grzybowski, M. Poliakoff, J.J. Turner and R.F. Turner, Inorg. Chem., 17 (1978) 147.
187 J.D. Black and P.S. Braterman, J. Am. Chem. Soc., 97 (1975) 2908.
188 J. Nasielski and A. Colas, J. Organometal. Chem., 101 (1975) 215.
189 M. Poliakoff, J. Chem. Soc. Faraday Trans. 2, 73 (1977) 569.
190 B. Davies, A. McNeish, M. Poliakoff, M. Tranquille and J.J. Turner, Chem. Commun., (1978) 36.
191 B. Davies, A. McNeish, M. Poliakoff, M. Tranquille and J.J. Turner, Chem. Phys. Lett., 52 (1977) 477.
192 R.T. Hall and G.C. Pimentel, J. Chem. Phys., 38 (1963) 1889.
193 J.K. Burdett, unpublished data.
194 W.G. Klemperer, J.K. Krieger, M.D. McCreary, E.L. Muetterties, D.D. Traficante and G.M. Whitesides, J. Am. Chem. Soc., 97 (1975) 7023.

58

195 P.H. Kasai, Phys. Rev. Lett., 21 (1968) 67.
196 D.E. Milligan and M.E. Jacox, J. Chem. Phys., 55 (1971) 3404.
197 R.C. Dunbar and B.B. Hutchinson, J. Am. Chem. Soc., 96 (1974) 3816.
198 J. Brauman, J.H. Richardson, and L.M. Stephenson, J. Am. Chem. Soc., 96 (1974) 3671.
199 R.L. Sweany and T.L. Brown, Inorg. Chem., 16 (1977) 415.
200 R.L. Sweany and T.L. Brown, Inorg. Chem., 16 (1977) 421.
201 J.K. Burdett, J.M. Grzybowski, M. Poliakoff and J.J. Turner, J. Am. Chem. Soc., 98 (1976) 5728.
202 R.K. Sheline and H. Mahnke, Angew. Chem. (Int. Ed. Engl.), 14 (1975) 314.
203 G.A. Ozin, Accounts Chem. Res., 10 (1977) 21,
204 O. Crichton and A.J. Rest, J. Chem. Soc. Dalton Trans., (1977) 536.
205 R.K. Sheline and J.L. Slater, Angew. Chem. (Int. Ed. Engl.), (1975) 309.
206 A.J.L. Hanlan and G.A. Ozin, Inorg. Chem., 16 (1977) 2848.
207 A.J.L. Hanlan and G.A. Ozin, Inorg. Chem., 16 (1977) 2857.
208 G.A. Ozin and W.J. Power, Inorg. Chem., 16 (1977) 2864.
209 G.A. Ozin, H. Huber and D. McIntosh, Inorg. Chem., 16 (1977) 3070.
210 M.J. Griffiths and R.F. Barrow, J. Chem. Soc. Faraday Trans. 2, (1977) 943.
211 S. Abramowitz, N. Aquista and I.W. Levin, Chem. Phys. Lett., 50 (1977) 423.
212 G.A. Ozin, H. Huber and D. McIntosh, Inorg. Chem., 17 (1978) 1472.